Award Number: DAMD17-01-1-0142

TITLE: Linking Sister Chromatid Cohesion to Apoptosis and Aneuploidy in the Development of Breast Cancer

PRINCIPAL INVESTIGATOR: Debananda Pati, Ph.D.

CONTRACTING ORGANIZATION: Baylor College of Medicine
Houston, TX 77030

REPORT DATE: July 2005

TYPE OF REPORT: Annual Summary

20060302 016

PREPARED FOR: U.S. Army Medical Research and Materiel Command
Fort Detrick, Maryland 21702-5012

DISTRIBUTION STATEMENT: Approved for Public Release;
Distribution Unlimited

REPORT DOCUMENTATION PAGE

Form Approved
OMB No. 0704-0188

1. REPORT DATE *(DD-MM-YYYY)*	2. REPORT TYPE	3. DATES COVERED *(From - To)*
01-07-2005	Annual Summary	1 Jul 2001 – 30 Jun 2005

4. TITLE AND SUBTITLE
Linking Sister Chromatid Cohesion to Apoptosis and Aneuploidy in the Development of Breast Cancer

5a. CONTRACT NUMBER

5b. GRANT NUMBER
DAMD17-01-1-0142

5c. PROGRAM ELEMENT NUMBER

6. AUTHOR(S)
Debananda Pati, Ph.D

E-Mail: pati@bcm.tmc.edu

5d. PROJECT NUMBER

5e. TASK NUMBER

5f. WORK UNIT NUMBER

7. PERFORMING ORGANIZATION NAME(S) AND ADDRESS(ES)

Baylor College of Medicine
Houston, TX 77030

8. PERFORMING ORGANIZATION REPORT NUMBER

9. SPONSORING / MONITORING AGENCY NAME(S) AND ADDRESS(ES)
U.S. Army Medical Research and Materiel Command
Fort Detrick, Maryland 21702-5012

10. SPONSOR/MONITOR'S ACRONYM(S)

11. SPONSOR/MONITOR'S REPORT NUMBER(S)

12. DISTRIBUTION / AVAILABILITY STATEMENT
Approved for Public Release; Distribution Unlimited

13. SUPPLEMENTARY NOTES

14. ABSTRACT
The purpose of this project is to identify effector molecules that act as a link between cell proliferation, cell survival and chromosomes stability. We have hypothesized that chromosomal segregation and apoptotic pathways are linked and have a role in breast cancer. Rad21 is one of the major cohesin subunits that holds sister chromatids together until anaphase, when proteolytic cleavage by separase allows chromosomal separation. Our study demonstrates that in contrast to described functions of Rad21, in chromosome segregation and DNA repair, cleavage of the cohesion protein and translocation of the C-terminal cleavage product to the cytoplasm are early events in the apoptotic pathway that amplify the apoptotic signal in a positive feed back manner by activating more Caspases. Overexpression of the c-terminal cleavage products results in apoptosis in MCF-7 breast cancer cells. Given the role of hRad21 in chromosome cohesion, the cleaved C-terminal product and its translocation to the cytoplasm may act as a nuclear signal for apoptosis. Furthermore, hRad21 is differentially expressed in human breast tumors and in breast cancer derived cell lines in comparison to normal breast epithelial cells. Future studies will identify the protease that cleaves Rad21 and evaluate hRad21 as a prognostic marker for breast cancer development.

15. SUBJECT TERMS
Pathobiology, cell cycle, apoptosis, aneuploidy, sister chromatid cohesion

16. SECURITY CLASSIFICATION OF:			17. LIMITATION OF ABSTRACT	18. NUMBER OF PAGES	19a. NAME OF RESPONSIBLE PERSON
a. REPORT	b. ABSTRACT	c. THIS PAGE			19b. TELEPHONE NUMBER *(include area code)*
U	U	U	UU	37	

Standard Form 298 (Rev. 8-98)
Prescribed by ANSI Std. Z39.18

Table of Contents

Introduction

One of the hallmarks of cancer cells is a decrease in or resistance to cell death coupled with an increase in cell proliferation. In particular, cancer cells can resist conventional chemotherapeutic agents by evading apoptosis. Therefore, a mechanistic understanding of the processes that link cell proliferation and cell death will provide important knowledge in the treatment of cancer. Cell death by apoptosis plays an essential role in normal development and physiology in the breast (Jacobson et al., 1997) as well as in the development of breast Cancer (Schedin et al., 1996; Wu, 1996). The degree of apoptosis can be an important factor in both the progression of breast cancer and the response to treatment (Furth, 1999; Lipponen, 1999). A high apoptotic index (number of apoptotic cells per square millimeter of neoplastic tissue) is related to malignant cellular features and is an indicator of invasiveness and cell proliferation in breast cancer (Lipponen, 1999). The response to treatment of breast cancer is improved by increasing the percentage of cells undergoing apoptosis. Thus, cell cycle progression and control of apoptosis are thought to be intimately linked processes. Mitosis and apoptosis are closely interrelated (Lipponen et al., 1994). Although proteins that regulate apoptosis have been implicated in restraining cell cycle entry (Hauf et al., 2001) and controlling ploidy (Minn et al., 1996), the effector molecules at the interface between cell proliferation and cell survival have remained elusive. **The purpose of the study is to identify the effector molecules that act as a link between cell proliferation, cell survival and chromosomal stability. We have hypothesized that chromosomal segregation and apoptotic pathways are linked and have a role in the development of aneuploidy in breast tumors. Human Rad21, a protein that establishes and maintains sister chromatid cohesion during mitosis, may provide a link between cell division and cell death: and cleavage of Rad21 may signal subsequent events of cell death including DNA degradation. We also hypothesize that hRad21 helps maintain chromosomal stability in mammary cells and its dysregulation results in breast cancer formation.** To test these hypotheses we have the following **specific aims:** 1) evaluate the role of hRad21 in the apoptotic response and the role of apoptotic proteins on cleavage of hRad21; and 2) determine the expression and localization of hRad21 protein and mRNA in normal and malignant breast carcinoma cell lines and tumor specimens with known levels of aneuploidy.

Following is the final report for this project that includes a no cost extension for the period of July 1, 2004-June 30-2005. We have completed the first technical objective (role of Rad21, in apoptotic response) and have made substantial progress in the second objective (Rad21 expression in breast tumors). Over the last year, with limited resources we just focused on the characterization of the protease that cleaves Rad21 during apoptotic response. Our other focus was to prepare and submit grant proposals to seek funding to continue this line of research. We have been successful in both of these goals. Our research indicates the presence of a novel Rad21 protease in the nucleus, which remains to be identified. Recently I have secured funding from NIH to carry out the identification and characterization of this novel Rad21 protease.

In summary, the research carried out as the part of this CDA award indicates that in addition to establishing and maintaining sister chromatid cohesion during mitosis, hRad21 plays a direct role in apoptosis, and its cleavage during apoptosis by a novel protease act as a nuclear signal to initiate cytoplasmic events involved in the apoptotic pathway. A manuscript describing this work (see Appendix III) was published in the *Journal of Molecular and Cellular Biology* (Pati et al., 2002), one manuscript is under revision and two more manuscripts are in preparation. In accordance with the approved statement of work, tasks for technical objective 1 and 2 have been completed (Appendix I).

Body of the report

Rad21 is one of the major cohesin subunits that holds sister chromatids together until anaphase, when proteolytic cleavage by separase, a caspase-like enzyme, allows chromosomal separation (Uhlmann et al., 1999; Biggins and Murray, 1999, Hauf et al., 2001). **Rad21 plays a critical role in the eukaryotic cell division cycle by regulating sister chromatid cohesion and separation at the metaphase to anaphase transition (Ciosk et al., 1998; Michaelis et al., 1997; Nasmyth et al., 2000). However, in addition to its role in chromosomal segregation, cohesins can associate with different sets of proteins to achieve diverse functions, including regulation of gene expression, DNA repair, cell cycle checkpoints and centromere organization (for a review see Hagstrom and Meyer, 2003). Surprisingly, work from ours and others have indicated that not only cohesin Rad21 plays a critical role in mitosis, it can also induce apoptosis (Pati et al., 2002, Chen et al., 2002).**
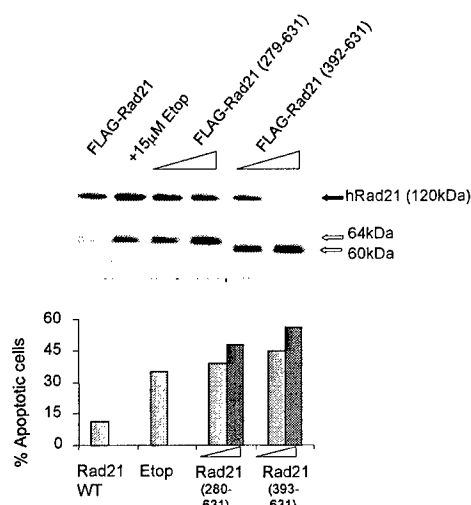
Fig: 1. Induction of cell death by cleaved Rad21 proteins (Rad21 280-631 and Rad21 393-631). Molt4 T-cells were transiently transfected with the plasmids encoding Rad21 WT (3 µg) or C-terminal cleavage products (3 and 6 µg), together with 3 µg of red fluorescent protein (RFP) expression plasmids. Total plasmid (9 µg) for each transfection was kept constant to avoid promoter competition. Forty-eight hours following transfection, RFP positive cells were evaluated by microscopy, and the percentage of RFP-positive cells with apoptotic morphology was estimated based on a count of 300 cells (Etop, etoposide).
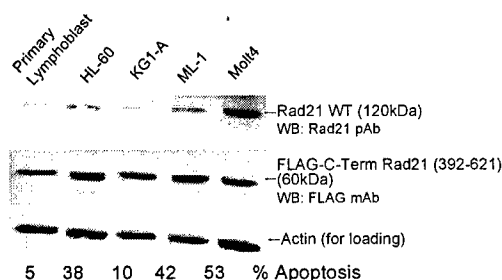

Fig. 2. Endogenous status of Rad21 protein influences C-terminal Rad2-induced apoptosis in normal lymphoblasts and myleoid leukemia cells. Cells were transfected with FLAG-tagged Rad21 together with an RFP expression plasmid using a combination of nucleofection (Amaxa Inc, Gaithersburg, MD) and lipid based transfection reagents from Qiagen (Valencia, CA) and Bio-Rad (Hercules, CA). Transfection efficiency was 15%-20%. 48 h posttransfection. Lysates were prepared and analyzed in Western blots using Rad21Ab, FLAG M2 mAb, and actin antiserum. A sample of RFP-positive cells were evaluated by microscopy, and the percentage of RFP-positive cells with apoptotic morphology was estimated by counting 300 cells.

Little is known about the role of Rad21 in human malignancies. We have characterized the role of Rad21 in apoptosis and have evaluated the expression of Rad21 in 800 human breast tumor specimens to identify its role in breast cancer progression.

Aim 1) Role of Rad21 in apoptotic response: Tasks completed as parts of this objective clearly demonstrate a role of hRad21 in the apoptotic response and cleavage of the hRad21 protein in human cells by a Caspase-like activity. Our published and recent unpublished studies demonstrate that Rad21 is cleaved during apoptosis at two unique sites (Asp residue 279 and Cysteine residue 392) and that the C-terminal cleavage products translocate to the cytoplasm where it enhances apoptosis. Moreover, overexpression of C-terminal Rad21 (280-631aa and 393-631aa) in the cytoplasm of apoptosis sensitive (e.g. MCF-7, Molt4) or resistant (293 cells) cell lines induces apoptosis in contrast to expression of full length or N-terminal (1-279aa) Rad21. Analysis of transfected 293T and Molt4 cells by multiple apoptosis assays, including cellular morphology under light microscopy and staining with TUNEL, Annexin V and DAPI, clearly indicate the ability of the 64-kDa C-terminal hRad21 to induce apoptosis. Using similar experimental approaches, we have now tested the effect of the 60-kDa hRad21 fragment (aa 393-631) on apoptosis. We found that like that of the 64-kDa Rad21, the 60-kDa Rad21 C-terminal fragment is also highly apoptotic. Quantitative analysis of Molt4 T-cells transfected with C-terminal hRad21 (aa 280-631 or aa 393-631) plasmids showed a dramatic increase in nuclear degradation compared with cells expressing wild-type hRad21 (pFLAG Rad21) (Fig. 1). The level of apoptosis in cells expressing the 60- or 64-kDa fragment is comparable to Molt4 cells treated with 15 µM etoposide for 6 h. In these cells, apoptosis was assayed by monitoring the phenotype of the DAPI-stained nuclei. Cells transfected with hRad21 C-terminal plasmids had considerably higher concentrations of cellular and nuclear phenotypes typical of apoptosis, such as having a round appearance with shrunken cell volume, chromatin condensation, and nuclear disintegration, than did cells with intact hRad21WT constructs.

Results indicate the proapoptotic activity of the C-terminal Rad21 fragments appears to rely on the endogenous status of Rad21 protein (Fig. 2). For example, when overexpressed, both the C-terminal fragments of Rad21 (60 kDa [Fig. 2, panel 2] and 64 kDa, [data not shown]) induce apoptosis in tumor cells with higher endogenous Rad21 levels (e.g., myeloid leukemia cells Molt4, ML-1, and HL60), while primary lymphocytes and tumor cells with low Rad21 expression (e.g. KG1A cells) are resistant, thus making Rad21 protein status an ideal target for therapy. This phenomenon may be due to:

(a) a hyperactive export mechanism that regulates the translocation of the pro-apoptotic Rad21 C-terminal fragment to the cytoplasm in Rad21 overexpressed cells or (b) an overactive Rad21-specific protease in cells with a high level of Rad21, resulting in higher Rad21 cleavage and translocation to cytoplasm.

We have further examined the importance of the proteolytic cleavage of Rad21 during apoptosis by engineering a Rad21 construct in which the endogenous apoptotic cleavage site is replaced by the TEV protease recognition sequence (TEV-Rad21). Expression of TEV-Rad21 alone had no effect on the cell cycle, where as co-expression of TEV-Rad21 with the highly specific TEV protease induced apoptosis in Jurkat and 293 cells (Fig. 3). In this assay, inclusion of TEV recognition site to other parts of Rad21 had no effect (data not shown). Thus,
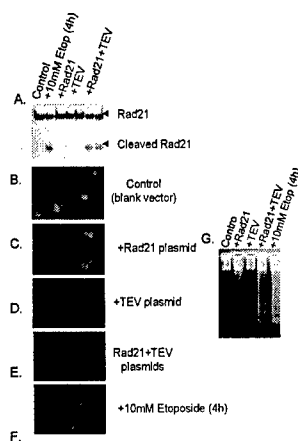
5

Fig.3. Cleavage of an engineered Rad21 that replaces the apoptotic cleavage site at Asp^{279} with a TEV protease recognition motif can induce apoptosis in Jurkat T cells. A Western blot analysis (A) of Jurkat cells (profiled in B through F) using Rad21 monoclonal antibody. Jurkat cells were transfected with blank vectors (B), treated with Rad21-engineered plasmid that replaced its apoptotic cleavage site with a TEV protease recognition sequence (C), treated with TEV expression plasmid (D), or treated with both Rad21 and TEV expression plasmids (E). As a control, cells were also treated with 10 μM etoposide for 4 h to induce apoptosis (F). Thirty-six hours following transfection, cells were fixed, stained with DAPI, and visualized using fluorescence microscopy. Transfection efficiency was 30%-40%. Assay of DNA fragmentation during Rad21 cleavage in Jurkat cells was also performed (G). In an identical set of experiments, cells were harvested and genomic DNA extracted from the cells and analyzed by 1.8% agarose gel electrophoresis. The DNA was visualized by UV illumination after Cyber Gold staining (Molecular Probes, Eugene, OR).
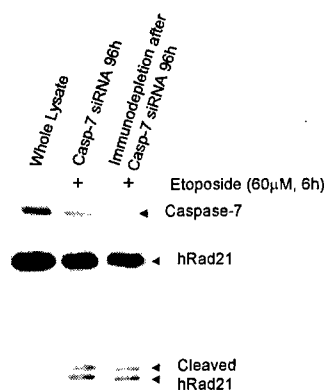
Fig. 4: Caspase 3 and 7 are not essential for the cleavage of hRad21. In vitro translated unlabeled (nonisotopic) Rad21 in wheat germ extract was incubated in the presence of MCF-7 whole cell lysate (no treatment) (left lane) or lysates that were immunodeplited using caspase 7 antibody from cells transfected with caspase 7 siRNA for 96 h and challenged with 60-μM etoposide, 6 h before harvest (lanes 2 and 3). Samples were resolved in 4%-20% gradient SDS-PAGE gel and immunoblot analyses were performed using caspase 7 and Rad21 monoclonal antisera. MCF-7 cells used here lack caspase 3.

cleavage of Rad21 close to its endogenous, apoptotic cleavage site is sufficient to induce apoptosis in both apoptosis sensitive and resistant cells. *In vitro* cleavage assays have indicated that caspase-3 and -7 can cleave Rad21. However, we recently have shown, that Rad21 can be cleaved in Caspase-3 deficient MCF7 cells in which Caspase-7 activity is blocked by siRNA/antibody treatment (Fig. 4).

Since Rad21 is a nuclear protein and the cleavage initially occurs in the nucleus, the protease that cleaves Rad21 may reside inside the nucleus. Caspase-2 is localized in nucleus (Shikama et al., 2001), but it cannot cleave Rad21 *in vitro* (Chen et al., 2002). These findings suggest the presence of a novel caspase or caspase-like molecule in the nucleus that cleaves Rad21 early in apoptosis. However, the physiological protease that cleaves Rad21 during apoptosis and the mechanisms by which apoptosis is promoted remains at present elusive.

Feasibility of the purification scheme to identify the protease that cleaves Rad21. To identify the physiological protease that cleaves Rad21 in the nucleus early in apoptosis, we undertook a set of pilot studies using Mono Q, an anion-exchange column, to isolate the enzymatically active fractions based on surface charge of the molecule, along with a BioLogic DuoFlow chromatography system (Bio-Rad, Hercules, CA). A Mono Q column contains quaternary amine groups and thus has a positive charge.
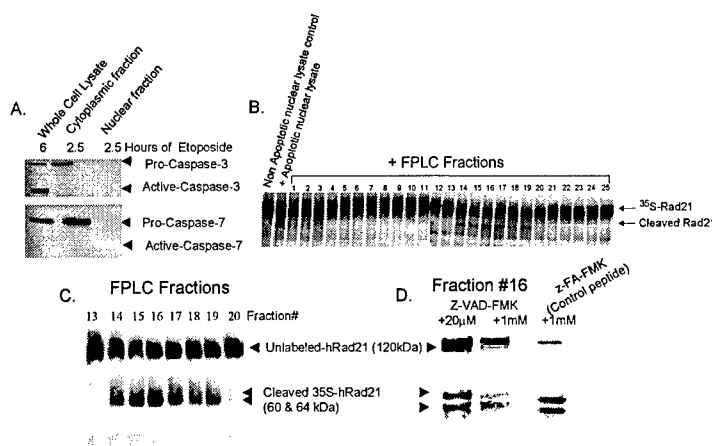

Fig. 5. Biochemical purification of active protease fractions that cleave hRad21 in vitro from nuclear lysates of Molt4 cells undergoing early apoptosis (10 μM etoposide treatment for 2.5 h), using preparative FPLC on a Mono Q column: (A) Assay for caspases 3 and 7 contamination of the nuclear fraction used for FPLC using Western blot analysis. Whole cell lysates (lane 1) from Molt4 cells treated with 10 μm etoposide for 6 h are shown as positive controls along with cytoplasmic fractions (lane 2). (B) In vitro translated ^{35}S-hRad21 in the rabbit reticulocyte lysates were incubated with nuclear lysates from Molt4 cells treated without etoposide (lane 1) and with 10 μM etoposide for 2.5 h (lane 2). Shown right are the FPLC-purified fractions of apoptotic nuclear lysates. Samples were resolved on a 12.5% SDS-PAGE gel, fixed with methanol and acetic acid for 30 min, dried on a gel dryer, and exposed to a Storm imager. (C) Cleavage of in vitro translated unlabeled (nonisotopic) hRad21 in wheat germ extracts by FPLC fractions 13-20. Samples were analyzed on an SDS-6% PAGE gel followed by Western bloting with hRda21 C-terminal pAb. (D) In vitro cleavage of unlabeled-Rad21 by FPLC fraction 16 in the presence of a broad-spectrum caspase inhibitor Z-VAD-FMK (20 μM and 1 mM) or a peptide control Cbz-Phe-Ala-fluoromethyl ketone (z-FA-FMK) (1 mM). .

Caspases are negatively charged molecules and should bind to the Mono Q column. In this experiment, 3 L of Molt4 cells were treated with 10 μM etoposide for 2.5 h. Quantitative measurement of early apoptosis was performed by staining a sample of cells following etoposide treatment with Annexin V as previously described (Pati et al., 2002). Isolation of nuclei was based on osmotic shock followed by sucrose gradient centrifugation. The

6

quality and density of the nuclei were monitored by staining of the nuclear material with DAPI and visualization using a hemocytometer. Our lab uses this method routinely to prepare nuclei from Molt4 cells with high purity (Pati et al., 2002). The purity of the nuclear fraction was verified in a Western blot using nuclear lamin and cytoplasmic tubulin antibodies and was found to be pure with no detectable cytoplasmic contamination (Pati et al., 2002). Although Western blot analysis was used to identify contamination of the nuclear preparations with cytoplasmic caspase 3 and caspase 7, two major apoptotic proteases, contamination was not detected (Fig. 5A).

Fast-performance liquid chromatography (FPLC) was used to purify nuclear lysates from early apoptotic Molt4 cells. Nuclear protein (500 mg at 1000 mg/ml) in buffer consisting of 10 mM Tris-HCL, 0.1 mM EDTA, 1 mM DTT (pH, 7.5), and 0.2 mM PMSF (buffer A) was applied to the Mono Q column, which had been equilibrated and developed with the same buffer. Then 0.75-ml fractions were collected and the enzymatic activity was tested in an in vitro ^{35}S-Rad21 cleavage assay as described previously (Pati et al., 2002). As shown in Fig. 5B, in vitro translated Rad21 was cleaved by the Molt4 nuclear lysates that were treated for 2.5 h with 10 µM etoposide (lane 2). However, control lysates treated solely with vehicle failed to cleave Rad21 in the cleavage assay (lane 1). FPLC fractions 14-19 were able to cleave Rad21 in the in vitro cleavage assay indicating the presence of active enzyme fractions, and the intensity of the cleavage bands' peak in fractions 16 and 17. We confirmed these findings using fractions 13-20 to cleave Rad21employing in vitro translated unlabelled hRad21 in wheat germ extracts and assaying the cleavage in Rad21 immunoblots (Fig. 5C). The broad-spectrum caspase inhibitor z-VAD-FMK, but **not** the control peptide z-FA-FMK, could inhibit the cleavage of the 64-kDa hRad21 fragment by FPLC fraction 16 at higher doses (1 mM), but it had no effect on the 60-kDa fragment (Fig. 5D). Because these findings suggest the involvement of a novel caspase-like protease, they support the hypothesis that a nuclear protease cleaves Rad21 early in apoptosis and can be isolated.

In future the identification and characterization of this novel protease should be carried out. Identification of this protease not only will shed light on the nuclear signal that initiates apoptosis, will also provide a ideal target for therapeutic intervention. These experiments were instrumental in identifying if Rad21 cleavage is essential for induction of apoptosis and/or sensitizes cells to undergo apoptosis after exposure to apoptotic agents.

Sequence mining indicates that a region of 104 amino acid residues in C-terminal Rad21 has high consensus (26% identities, 43% positives) with the sequence upstream of the death domain (DD) of several apoptosis related proteins (Fig. 6), such as Tumor Necrosis Factor (TNF) receptor super family, apoptosis inducing receptor TRAIL-R2, and apoptosis inducing protein/death receptor 5 (Schneider et al 1997, Screaton et al 1997, Sheridan et al 1997, Walczak et al 1997). However, the functional significance of this domain in apoptosis-inducing proteins is not known. TNF receptor superfamily members have DD and their involvement in apoptosis requires TNF signaling from outside of the cell. C-terminal Rad21 does not have a death domain. It is currently not known whether C-terminal Rad21 induced apoptosis requires extracellular signals, like those in the TNF superfamily. **The conserve sequence between C-terminal Rad21 and TNF receptor superfamily members implies that Apoptosis induced by C-terminal Rad21 and the tumor necrosis factor (TNF) receptor superfamily may share part of the common apoptotic pathway.**

```
Rad21      ........MDE...NVS.GG.DS-..SVDP..PMPTM.DQTT.V.N.E.AFA.E..IDITVK.TKAKR..K..VD.VKELD.K...AQLS...........TTLDLA..PT.K.
AIP        ........NVL...VS.LQ.TQV..QEME.V.EPAEP.GVNM.S.G.S.HL-..A-----.AERSQ.RRLLV..NEGDP.E....QCFD...ADL..PFDSWE..LM.R.
consensus  + P+ +D    ++ VS+  P   P+    V+      T    L P E E   LEP     E     +R+L+V +     + T+R    D++D+V     P   +KL
```

Fig.6 Homology of C-terminal human Rad21 (amino acids 257-360) with apoptosis-inducing proteins (AIP) that include tumor necrosis factor receptor superfamily (member 10b, amino acids 188-286), apoptosis inducing receptor TRAIL-R2 (amino acids 263-361), and apoptosis inducing protein/death receptor 5 (amino acids 234-332). All these apoptosis-inducing proteins have a region with the same amino acid sequence.

To characterize the role of this identified AIP domain in C-terminal Rad21, we have set up a Hela Tet-On gene expression systems conditionally expressing Rad21 full length, Rad21(1-282aa), Rad21(281-631aa) and Rad21(253-631aa). Gene expression in Tet-on system is turned on by adding doxycycline and is tightly regulated in response to varying concentrations of doxycycline. These inducible cell lines are important reagent to study the C-terminal Rad21 stimulated apoptosis. We have also generated similar systems for the MCF7 breast cancer cell line, which will be used in testing C-terminal Rad21-induced apoptosis in breast cancer cells and will provide a valuable tool to probe the apoptotic activity of Rad21.

Aim 2) Expression and localization of Rad21 Protein and mRNA in normal and malignant breast carcinoma cell lines and tumor samples:

We have examined the expression pattern of Rad21message and protein in a variety of breast cancer cell lines (MCF7, MDA-MB-157, MDA-MB-231, MDA-MB-436, BT-20, HBL100, and SKBR-3. In these cells, Rad21 appeared to have altered expression patterns. Compared to normal human mammary epithelial cells (H-MEC), Rad21 mRNA is overexpressed in all the cells tested, except for BT20, where its expression was found to be considerably down regulated. However, subsequent Southern blot analysis of the genomic DNA from the breast cancer cell lines didn't reveal any defects in Rad21 gene structure. Expression and localization of the hRad21 protein in normal and malignant breast cancer cells were performed using immunocytochemistry and immunofluorescence techniques. hRad21 efficiently localizes to the nucleus of various mammalian cells assayed by immunofluorescence staining using either the affinity purified polyclonal or monoclonal hRad21 antibodies, developed by us.
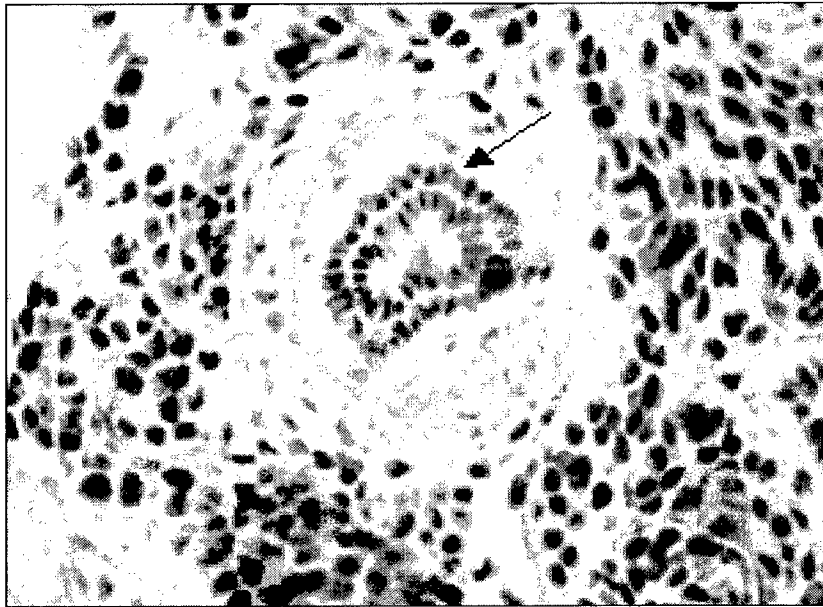

Fig. 7: Immunohistochemical staining of Rad21 in human breast tumor specimen. The signal was developed using 3,3'-diaminobenzidine chrmogen (brown) with a methyl green counter stain. In the center shows normal tissue (arrow). X100 maginification.

To further characterize the contribution of Rad21 to tumor localization of Rad21 protein, we used immunohistochemistry (Allred et al., 1993; Berardo et al., 1998) in 800 human breast tumor specimens with known status for aneuploidy, estrogen receptor, and a number of other markers with appropriate controls available from the Allred lab at the Baylor Breast Cancer Center. The Allred lab has assisted us in developing a robust assay to immunolocalize the hRad21 protein using monoclonal hRad21 antibody. Since most referral specimens are fixed 10% neutral buffered formalin and processed at variable rates and times, increased sensitivity and standardization of the assay is achieved through the use of heat induced antigen retrieval post–deparaffinization. Endogenous nonspecific protein blocking then follows. Subsequently, incubation with the primary antibody (monoclonal hRad21) is performed, followed by a biotinylated secondary antibody incubation directed against the mouse. These are then followed by incubation in horseradish peroxidase (HRP)-labeled streptavidin, which then binds to the biotin label of the secondary antibody. The entire reaction is then visualized by incubation with 3,3 diaminobenzedine which, in the presence of HRP, produces a brown reaction product at the site of the antigen-antibody interaction. Enhancement of the reaction product is achieved by the addition of the heavy metal osmium tetroxide, which increases the tone of the reaction product and elevates the signal: noise ratio of the assay. Scoring of immunostained slides for hRad21 expression is preformed by the PI in a blinded way according to the protocol described for Bcl-2 expression in breast tumor specimens (Berardo et al., 1998) and based on the proportion of cells staining positive, described by the Allred laboratory. Statistical analysis of these samples have been completed by the statistics core

(S.G. Hilsenbeck and C.C. Chenault) of the Breast Center at Baylor College of Medicine. Analysis indicates aberrant expression of Rad21 in human breast tumors. For an example, in one set of tumors Rad21 is highly overexpressed while in another set its expression is completely absent. There appears to be a high correlation between Rad21 expression in tumor and adjacent cells. Typically, Rad21 find to be expressed higher in infiltrating breast cancer (IBC) than in normal. The p value ($P<0.001$) indicated a highly significant difference. No obvious association was noted between ploidy of tumor and Rad21 expression in tumor tissues. However, it appears that there is an association between tumor ploidy and the expression of Rad21 in adjacent normal tissues that is statistically significant. There is a modest association between Rad21 and ER positivity in IBC but not in normal tissue. There was no significant association between Rad21 expression with cathepsin-D, her2-neu and EGFR. Due to lack of availability of enough sample materials, we were not able to perform the TUNEL assay as proposed to correlate the apoptotic index with Rad21 expression in these specimens. Based on these results, in future studies Rad21 can be evaluated as a potential candidate prognostic marker for breast cancer progression.

Due to difficulty in isolating RNA from frozen tumor specimens, expressions of *hRAD21* mRNA was being investigated in a subset of 10 breast tumors with Northern blot analysis. However, due to poor quality of the RNA, Northern analysis of Rad21 expression was not successful. The LOH studies (technical objective 2B) were proposed in collaboration with Dr. Peter O'Connell. This collaboration could not materialized partly due to the relocation of the O'Connell lab and partly due to lack of samples. Hence, this sub-aim was not pursued.

As described above, studies in over 800 human breast tumor specimen indicate that Rad21 is significantly overexpressed in human breast cancer cells in comparison to normal cells (Fig. 7, Zhang, Allred and Pati, manuscript in preparation), making it an attractive candidate for the adoptive immunotherapy with antigen-specific cytotoxic T-lymphocytes (CTL). Rad21 has also been reported to be amplified in prostrate cancer (Porkka et al., 2004). Rad21 is a potential tumor-associated self antigen similar to survivin, telomerase and MDM2 (Gordan et al., 2002). CTL specific for survivin and telomerase have been generated by several groups indicating that CTL can be successfully generated against self-antigens. Moreover, studies with survivin-specific CTL have shown that only tumor cells overexpressing survivin are recognized by CTL in contrast to non-malignant cells, likehematopoietic stem cells that express survivin at low levels (Pisarev et al., 2003). Thus, we hypothesize that Rad21-specific CTL will only recognize Rad21 overexpressing malignant cells. Sofar the immune response to Rad21 has not been studied and we have recently secured seed funds from the Baylor Cancer Center to generate Rad21-specific CTL for the adoptive immunotherapy of Rad21 positive breast cancer.

Mechanism of Hormone induced Aneuploidy: Over the last year I have embarked upon a new project to study the mechanism of steroid hormone induced aneuploidy in p53 null mammary epithelium. The absence of p53 function increases risk for spontaneous tumorigenesis in the mammary gland. Hormonal (estrogen and progesterone) stimulation enhances tumor risk in p53-null mammary epithelial cells as well as the incidence of aneuploidy. Aneuploidy appears in normal p53-null mammary epithelial cells within 5 weeks of hormone stimulation. In collaboration with Dr. Daniel Medina's laboratory at Baylor College of Medicine we investigated a possible mechanism of hormone-induced aneuploidy. Hormones increased DNA synthesis equally between wild-type (WT) and p53-null mammary epithelial cells. There were two distinct responses in p53-null cells to hormone exposure. First, Western blot analysis demonstrated that the levels of two proteins involved in regulating sister chromatid separation and the spindle checkpoint, Mad2 and separase (ESPL1) were increased in null compared with WT cells. In contrast, the levels of securin and Rad21 proteins were not increased in hormone-stimulated p53-null compared with WT cells. ESPL1 RNA was also increased in p53-null mouse mammary cells in vivo by 18 h of hormone stimulation and in human breast MCF7 cells in monolayer culture by 8 h of hormone stimulation. Furthermore, both promoters contained p53 and steroid hormone response elements. Mad2 protein was increased as a consequence of the absence of p53 function. The increase in Mad2 protein was observed also at the cellular level by immunohistochemistry. Second, hormones increased gene amplification in the distal arm of chromosome 2, as shown by comparative genomic hybridization. These results support the hypothesis that hormone stimulation acts to increase aneuploidy by several mechanisms. First, by increasing mitogenesis in the absence of the p53 checkpoint in G2, hormones allow the accumulation of cells that have experienced chromosome missegregation. Second, the absolute rate of chromosome missegregation may be increased by alterations in the levels of two proteins, separase and Mad2, which are important for maintaining chromosomal segregation and the normal spindle checkpoint during mitosis. This work was published in Cancer Research (Pati et al., 2004). Recently, I have also secured funding from Susan G. Komen Foundation and from NIH in the form of a RO1 grant to study further the molecular basis of aneuploidy in breast cancer.

Key Research Accomplishments

- Human Rad21 (hRad21) cohesin is cleaved at residue Asp (D)^{279} and Cys-392 (C^{392}) by a novel Caspase-like protease in the nucleus early in apoptotic process. The cleaved carboxy-terminal products are translocated to the cytoplasm early in apoptosis before chromatin condensation and nuclear fragmentation.
- Cleavage of Rad21 close to its endogenous, apoptotic cleavage site is sufficient to induce apoptosis in both apoptosis sensitive and resistant cells providing a direct and novel role of Rad21 in apoptosis.
- Overexpression of the 60 and 64 kDa cleavage product results in apoptosis in MCF-7 breast cancer cells. Given the role of hRad21 in chromosome cohesion, the cleaved C-terminal product and its translocation to the cytoplasm may act as a nuclear signal for apoptosis.
- Studies show that Rad21 can be cleaved in Caspase-3 deficient MCF7 cells in which Caspase-7 activity is blocked by siRNA/antibody treatment suggest that Caspase-3 and -7 are not the essential proteases that cleave Rad21. Since Rad21 is a nuclear protein and the cleavage initially occurs in the nucleus, the protease that cleaves Rad21 may reside inside the nucleus. Caspase-2 is localized in nucleus, but it cannot cleave Rad21 *in vitro*. These findings suggest the presence of a novel Caspase or Caspase-like molecule in the nucleus that cleaves Rad21 early in apoptosis.
- hRad21 is overexpressed in human breast tumors and in a number of breast cancer derived cell lines in comparison to normal breast epithelial cells. There appears to be a positive correlation between tumor ploidy and expression of Rad21 in the adjacent normal tissues.

Reportable Outcomes
Manuscript:

Pati, D*., Zhang, N., and Plon, S.E. (2002). Linking sister chromatid cohesion to apoptosis: role of Rad21. *Molecular and Cellular Biology* 22: 8267-8277. (*** Corresponding author**).

Pati, D., Haddad, B. R., Haegele, A., Thompson, H., Kittrell, F.S., Shepard, A., Montagna, C., Zhang, N.G., Ge, G., Otta, S. K. , McCarthy, M., Ullrich, R.L., and Medina, D. (2004). Hormone-induced chromosomal instability in p53 null mammary epithelium. *Cancer Research*. 64(16):5608-16.

Manuscript in Revision:

Zhang, N, Li, K, and **Pati, D.** A new model for sister chromatid cohesion in mammalian cells.

Manuscripts in Preparation:
Zhang, N., Allred, D.C.and **Pati, D.** Amplification of Rad21 in human breast cancer.

Pati, D. Role of chromosomal segregation proteins in apoptosis: Identification of a novel pathway.

Employment:
Four summer studentships were granted to Ulysses Burley (2002), Jessica S. Ross (2003), Alexander Rancier (2004), and Sidney Adeleke (2005) undergraduate students of Morehouse College, Fayetteville State University, Houston-Tillotson College, and Houston Baptist University respectively by the SMART program of Baylor College of Medicine to work on this project. SMART program is funded by the National Institute of Heath, National Institute of General Medical sciences.

Funding:

Based on the results obtained from these studies I was successful in securing following grants:

1) R01 (Pati)   12/1/2005 – 11/30/2010
NIH/NCI   Priority score 166 (percentile 8.8)
Mitotic regulation of apoptosis in leukemia

2) 2005 Cancer Center Pilot Project Award (Pati)   7/1/2005 – 6/30/2007
Chromosomal Cohesin Protein Rad21 as a Novel Therapeutic Target for Breast Cancer

3) Susan G. Komen Foundation (Pati)   05/01/05 - 04/30/07
Research Grant
Role of Separase in Breast Cancer

4) 1) R01 (Pati)   12/1/2005 – 11/30/2010
NIH/NCI   Priority score 150 (percentile 10.5)
Molecular basis of aneuploidy

Conclusion

In summary, in contrast to previously described functions of Rad21, in chromosome segregation and DNA repair, cleavage of the cohesion protein and translocation of the C-terminal cleavage products to the cytoplasm are early events in the apoptotic pathway that amplify the apoptotic signal in a positive feed back manner by activating more Caspases. It is apparent that cohesin Rad21 may act as an interface between cohesion and cell death, and its cleavage may signal subsequent events of apoptosis. These results provide the framework for establishing a link between sister chromatid cohesion and the apoptotic response that have not previously been tested in any model system. Furthermore, our studies indicate overexpression of Rad21 protein in human breast tumor specimens. Future studies will identify the physiological protease that cleaves Rad21 and role of hRad21 in the apoptotic response in normal and malignant cells.

References

Allred, D.C., Clark, G.M., Randon A.K., McGuire, W.L. Immunohistochemistry on histological sections from small (50mg) samples of pulverized breast cancer. *Histotech*, **16**: 117-120 (1993).

Berardo, M.D., Elledge, R.M., Moor C.D., Clark, G.M., Osborn, C.K., Allred, D.C. bcl-2 and apoptosis in lymph node positive breast carcinoma. *Cancer*, **82**: 1296-1302 (1998).

Biggins, S., Murray, A.W. Sister chromatid cohesion in mitosis. *Current opinion in Genetics and Development*, **9**: 230-236 (1999).

Chen, F., Kamradt, M., Mulcahy, M., Byun, Y., Xu, H., Mckay, M.J., Cryns, V.L. Caspase proteolysis of the cohesin component Rad21 promotes apoptosis. *J Biol Chem* **277**:16775-81 (2002).

Ciosk, R., Zachariae, W. Michaelis, C., Shevchenko, A., Mann, M., Nasmyth, K. An ESP1/PDS1 complex regulates loss of sister chromatid cohesion at the metaphase to anaphase transition in yeast. *Cell,* **93**: 1067-1076 (1998).

Furth, P.A. Apoptosis and the development of breast cancer. In "Breast Cancer: Molecular Genetics, Pathogenesis, and Therapeutics" (Eds. A. M. Bowcock and N. J. Towowa), Humana Press, NY, p171-180 (1999).

Gordan JD, Vonderheide RH. Universal tumor antigens as targets for immunotherapy. *Cytotherapy*. **4**:317-327 (2002).

Hagstrom, K.A., and Meyer, B.J. Condensin and cohesin: more than chromosome compactor and glue, *Nature Reviews, Genetics* **4**: 520-534 (2003).

Hauf, S., I. C. Waizenegger, and J-M. Peters. Cohesin cleavage by separase required for anaphase and cytokinesis in human cells. *Science*, **293**:1320-1323 (2001).

Huang, D.C.S., O'Reilly, L.A. Strasser, A., Cory, S. The anti-apoptosis function of bcl-2 can be genetically separated from its inhibitory effect on cell cycle entry. *EMBO J.,* **16**: 4628-4638 (1997).

Jacobson, M.D., Weil, M., Raff, M.C. Programmed cell death in animal development. *Cell*, **88**: 347-354 (1997).

Lipponen, P. Apoptosis in breast cancer: relationship with other pathological parameters. *Endocrine Related Cancer*, **6**: 13-16 (1999).

Lipponen, P., Aaltomaa, S., Kosma, V-M., Syrjanen, K. Apoptosis in breast cancer as related to histopathological characteristics and prognosis. *European Journal of Pathology*, **30A**: 2068-2073 (1994).

Michaelis, C., Ciosk, R., Nasmyth, K. Cohesins: Chromosomal proteins that prevent premature separation of sister chromatids. *Cell*, **91**: 35-45 (1997).

Minn, A.J., Boise, L.H., Thompson, C.B. Expression of Bcl-X_l and loss of p53 can cooperate to overcome a cell cycle checkpoint induced by mitotic spindle damage. *Genes Dev.,* **10**: 2621-2631 (1996).

Nasmyth, K., Peters, J.M., Uhlmann, F. Splitting the Chromosome: Cutting the Ties That Bind Sister Chromatids. *Science,* **288**: 1379-1385 (2000).

Pati, D., Zhang, N., Plon, S.E. Linking Sister Chromatid Cohesion and Apoptosis: Role of Rad21 *Molecular and Cellular Biology* **22**: 8267-8277 (2002)

Pati, D., Haddad, B. R., Haegele, A., Thompson, H., Kittrell, F.S., Shepard, A., Montagna, C., Zhang, N.G., Ge, G., Otta, S. K. , McCarthy, M., Ullrich, R.L., and Medina, D. Hormone-induced chromosomal instability in p53 null mammary epithelium. *Cancer Research.* **64**(16):5608-16 (2004).

Pisarev V, Yu B, Salup R et al. Full-length dominant-negative survivin for cancer immunotherapy. *Clin Cancer Res.***9**:6523-6533 (2003).

Porkka KP, Tammela TL, Vessella RL, Visakorpi T. RAD21 and KIAA0196 at 8q24 are amplified and overexpressed in prostate cancer. *Genes Chromosomes Cancer.* **39**(1):1-10 (2004).

Schedin, P.J., Thackray, L.B., Malone, P., Fontaine, S.C., Friis, R.R. Strange, R. Programmed cell death and mammary neoplasia. *Cancer. Treat. Res.*, **83**: 3-22 (1996).

Schneider, P., Bodmer, J.L., Thome, M., Hofmann, K., Holler, N., Tschopp, J. Characterization of two receptors for TRAIL. *FEBS Lett* **416**:329-34 (1997).

Schwarze, S.R., and Dowdy, S.F. In vivo protein transduction: intracellular delivery of biologically active proteins, compounds and DNA. *Trends in Pharmacological Sciences*, **21**: 45-48 (2000).

Screaton, G.R., Mongkolsapaya, J., Xu, X.N., Cowper, A.E., McMichael, A.J., Bell, J.I. TRICK2, a new alternatively spliced receptor that transduces the cytotoxic signal from TRAIL. *Curr Biol* 7:693-6 (1997).

Sheridan, J.P., Marsters, S.A., Pitti, R.M., Gurney, A., Skubatch, M., Baldwin, D., Ramakrishnan, L., Gray, C.L., Baker, K., Wood, W.I., Goddard, A.D., Godowski, P., Ashkenazi, A. Control of TRAIL-induced apoptosis by a family of signaling and decoy receptors. *Science* **277**:818-21 (1997).

Shikama Y, U M, Miyashita T, Yamada M. Comprehensive studies on subcellular localizations and cell death-inducing activities of eight GFP-tagged apoptosis-related caspases. *Exp Cell Res.* **264**:315-325 (2001).

Uhlmann, F., Lottspeich, F., Nasmyth, K. Sister chromatid separation at anaphase onset is promoted by cleavage of the cohesin subunit Scc1, *Nature*, **400**: 37-42 (1999).

Walczak, H., Degli-Esposti, M.A., Johnson, R.S., Smolak, P.J., Waugh, J.Y., Boiani, N., Timour, M.S., Gerhart, M.J., Schooley, K.A., Smith, C.A., Goodwin, R.G., Rauch, C.T. TRAIL-R2: a novel apoptosis-mediating receptor for TRAIL. *EMBO J* 16:5386-97 (1997).

Wu, J. Apoptosis and angiogenesis: two promising tumor markers in breast cancer. *Anticancer Research*, **16**: 2233-9 (1996).

Appendix-I
Statement of Work
(Work accomplished)

Technical Objective 1:

Month	Task	Status
1-4	Assessment of hRad21 cleavage and its immunolocalization in breast cancer cells after induction of apoptosis with DNA-damaging, non-DNA-damaging agents and microtubule-damaging drugs. Construction of mutant hRad21 expression constructs	**Completed**

Technical Objective 1A:

Month	Task	Status
5-9	Development of a *in vitro* cleavage assay for hRad21 and *in vivo* assay for Caspase activity and Caspase inhibitor studies	**Completed**
6-10	Mapping of the Rad21 cleavage site	**Completed**

Technical Objective 1B:

Month	Task	Status
9-12	Construction of pTAT-hRad21 and pTAT-cleaved hRad21 expression plasmids. Expression and isolation of recombinant Tat-Rad21 fusion protein	**Completed**
13-18	Tansduction of TAT-hRad21 into mammary cells Cell cycle analysis, aneuploidy status and apoptosis assay of transduced cells	**Completed**

Technical Objective 1C:

Will not be carried out. A study published recently from another lab has performed similar experiments proposed in this objective. In this study by Chen et al. (2002) have examined the role of survivin on Rad21-induced apoptosis. These studies indicated that Rad21-induced apoptosis can be inhibited by anti-apoptotic proteins such as Survivin.

Technical Objective 2A & 2B:

Month	Task	
10-16	Southern blot analysis of *hRAD21* gene in breast cancer cell lines	**Completed**
12-42	LOH and mutational studies	**Abandoned.**

Technical Objective 2C & 2D:

Month	Task	
1-4	Isolation of RNA, DNA and protein from breast tumor samples	**Completed**
5-12	Immunohistochemical localization and detection of Rad21 in human breast tumor sections	**Completed**
8-18	Northern and Western analysis of hRad21 transcripts and protein	**Completed**

expression in breast tumor specimens.

12-30   Detection of apoptosis and aneuploidy in relation to Rad21 expression in breast tumor specimens
Abandoned due to technical difficulties.

42-48   Preparation of annual reports and manuscripts. Preparation of grant applications for future funding.
Completed.

Appendix-II
Bibliography of all publications and Meeting Abstracts

Journal Article:
Pati, D*., Zhang, N., and Plon, S.E. (2002). Linking sister chromatid cohesion to apoptosis: role of Rad21. *Molecular and Cellular Biology* **22**: 8267-8277. (* **Corresponding author**).

Pati, D., Haddad, B. R., Haegele, A., Thompson, H., Kittrell, F.S., Shepard, A., Montagna, C., Zhang, N.G., Ge, G., Otta, S. K., McCarthy, M., Ullrich, R.L., and Medina, D. (2004). Hormone-induced chromosomal instability in p53 null mammary epithelium. *Cancer Research*. 64(16):5608-16.

Meeting Abstract:
Pati, D., and Plon, S.E. (2002). Linking sister chromatid cohesion to apoptosis: role of hRad21. Abstract book of the Cell Cycle meeting, Cold Spring Harbor Laboratory, New York, May15-19, 2002, p153.

Zhang NG, Ge G, Kittrell FC, Otta SK, Medina D, **Pati D**. (2004) Interaction of separase, p53 and steroids: new Insights into the mechanisms of hormone-induced aneuploidy. Abstract book of the Cell Cycle meeting, Cold Spring Harbor Laboratory, New York. May 19-23, 2004, p193.

Appendix-III (Published Manuscript)

Linking Sister Chromatid Cohesion and Apoptosis: Role of Rad21

Debananda Pati,* Nenggang Zhang, and Sharon E. Plon

Texas Children's Cancer Center, Department of Pediatrics, Baylor College of Medicine, Houston, Texas 77030

Rad21 is one of the major cohesin subunits that holds sister chromatids together until anaphase, when proteolytic cleavage by separase, a caspase-like enzyme, allows chromosomal separation. We show that cleavage of human Rad21 (hRad21) also occurs during apoptosis induced by diverse stimuli. Induction of apoptosis in multiple human cell lines results in the early (4 h after insult) generation of 64- and 60-kDa carboxy-terminal hRad21 cleavage products. We biochemically mapped an apoptotic cleavage site at residue Asp-279 (D^{279}) of hRad21. This apoptotic cleavage site is distinct from previously described mitotic cleavage sites. hRad21 is a nuclear protein; however, the cleaved 64-kDa carboxy-terminal product is translocated to the cytoplasm early in apoptosis before chromatin condensation and nuclear fragmentation. Overexpression of the 64-kDa cleavage product results in apoptosis in Molt4, MCF-7, and 293T cells, as determined by TUNEL (terminal deoxynucleotidyltransferase-mediated dUTP-biotin nick end labeling) and Annexin V staining, assaying of caspase-3 activity, and examination of nuclear morphology. Given the role of hRad21 in chromosome cohesion, the cleaved C-terminal product and its translocation to the cytoplasm may act as a nuclear signal for apoptosis. In summary, we show that cleavage of a cohesion protein and translocation of the C-terminal cleavage product to the cytoplasm are early events in the apoptotic pathway and cause amplification of the cell death signal in a positive-feedback manner.

Normal development and homeostasis require the orderly regulation of both cell proliferation and cell survival. Cell cycle progression and control of apoptosis are thought to be intimately linked processes. Activation of the cell cycle plays a significant role in the regulation of apoptosis (16); in some cell types and under certain conditions, apoptosis has been shown to occur only at specific stages of the cell cycle (24). Mitosis and apoptosis are also closely interrelated (25), and the mitotic index is the most important determinant of the apoptotic index (25). Although proteins that regulate apoptosis have been implicated in the restraint of cell cycle entry (14) and the control of ploidy (29), the effector molecules at the interface between cell proliferation and cell survival have remained elusive.

Studies with yeast and higher eukaryotes, including humans, have indicated that an evolutionarily conserved protein complex, called cohesin, and its subunit, Mcd1/Scc1/hRad21, are required for appropriate arrangement of chromosomes during normal cell division (11, 28; for a review, see references 20, 30, 31, and 36). Analyses of Rad21 function in fission yeast, *Schizosaccharomyces pombe*, and of Scc1/Mcd1 function in budding yeast, *Saccharomyces cerevisiae*, have demonstrated that the nuclear phosphoprotein is required for appropriate chromosomal cohesion during the mitotic cell cycle and double-strand-break repair after DNA damage (1, 30). Biochemical analysis of cohesin indicates that it acts as a molecular glue, and human cohesin can promote intermolecular DNA catenation, a mechanism that links two sister chromatids together (26). In budding yeast, loss of cohesion at the metaphase-anaphase transition is accompanied by proteolytic cleavage of the Scc1/Mcd1 protein (11, 28, 30, 37) followed by its dissociation from the

chromatids (28, 30). Cleavage depends on a CD clan endopeptidase, Esp1 (also known as separin/separase) (37, 38), which is complexed with its inhibitor, Pds1 (securin), before anaphase (23, 39). In metaphase, ubiquitin-mediated degradation of the securin protein by APC/C-Cdc20 ubiquitin-ligase releases separin protein, which proteolytically cleaves cohesin Rad21, thereby releasing the sister chromatids (6, 7, 10, 18, 42). In budding yeast, fission yeast, and human cells, Rad21 has two mitotic cleavage sites for separase (12, 37, 38), and cleavage by separase appears to be essential for sister chromatid separation and for the completion of cytokinesis (12). In contrast to the simultaneous release of cohesin from the chromosome arms and centromere region in budding yeast by separase cleavage, most cohesin in metazoans is removed in early prophase from chromosome arms by a cleavage-independent mechanism (12, 39, 40). Only residual amounts of cohesin are cleaved at the onset of anaphase, coinciding with its disappearance from centromeres. Thus, Scc1/Mcd1/Rad21 plays a critical role in the eukaryotic cell division cycle by regulating sister chromatid cohesion and separation at the metaphase-to-anaphase transition.

Our results indicate that in addition to establishing and maintaining sister chromatid cohesion during mitosis, hRad21 plays a role in apoptosis, and its cleavage during apoptosis may act as a nuclear signal to initiate cytoplasmic events involved in the apoptotic pathway.

MATERIALS AND METHODS

Plasmids. Full-length *hRAD21* cDNA plasmid (KIAA 0078) in pBluescript SK(+) vector was obtained from Kazusa DNA Research Institute, Chiba, Japan. Full-length *hRAD21* cDNA was subcloned into several mammalian expression plasmids, including pFLAGCMV2, pCS2MT, and pCDNA6Myc-HisC, to produce epitope-tagged proteins where applicable. *hRad21* cDNA was also subcloned in frame upstream of the *myc* epitope in pCMV/*myc*/Nuc and pCMV/*myc*/Cyto (Invitrogen, Carlsbad, Calif.) to direct the expression of hRad21 protein to the nucleus and cytoplasm, respectively. The following plasmids were

* Corresponding author. Mailing address: Texas Children's Cancer Center, Baylor College of Medicine, 6621 Fannin St., MC 3-3320, Houston, TX 77030. Phone: (832) 824-4575. Fax: (832) 825-4202. E-mail: pati@bcm.tmc.edu.

used for transfection: pCS2MT-*hRAD21* was constructed by in-frame ligation of the 2,331-bp *NcoI/DraI* fragment bearing the *hRAD21* cDNA to the end of the sixth *myc* epitope in pCS2MT (B. Kelley, Fred Hutchinson Cancer Center, Seattle, Wash.); pFLAGCMV2-*hRAD21* was generated by cloning the full-length *hRAD21* gene contained on a 2,578-bp *MscI/StuI* fragment from pSKKIAA0078 into pFLAGCMV2 (Kodak) that was digested with *SmaI*.

Site-directed mutagenesis of hRad21. pCS2MT-*hRAD21* apoptotic cleavage site (ACS) mutants I (PDSPD^{279}S to PDSPA^{279}S) and II (PD^{276}S^{277}PD^{279}S^{280} to PA^{276}A^{277}PA^{279}A^{280}) were generated using a PCR-based site-directed mutagenesis protocol as previously described (33). The PCR resulted in a 550-bp internal *hRAD21* fragment containing the mutations. A 221-bp piece of wild-type (WT) *hRAD21* (from the *BsgI* to PFLFI sites) was replaced with the comparable mutated fragment. The resulting plasmids, pCS2MT-*hRAD21*-ACS-mut-I and pCS2MT-*hRAD21*-ACS-mut-II, were verified by DNA sequencing. The amino-terminal (N-hRad21, encoding amino acids [aa] 1 to 279) and carboxy-terminal (C-hRad21, encoding aa 280 to 631) cleavage products were cloned into *myc* epitope-tagged pCS2MT vectors by using PCR amplification of the fragments from the *hRAD21* cDNA. These constructs were also verified by DNA sequencing.

Generation of hRad21 pAb and mAb. Rabbit polyclonal antibody (pAb) was raised commercially (Covance, Denver, Pa.) against synthetic peptides corresponding to the sequence of the 14 carboxy terminal aa of hRad21 (SDIIAT-PGPRFHII). Immunization and affinity purification of antibodies were performed according to the manufacturer's protocol. Monoclonal antibody (mAb) against a partial recombinant hRad21 protein (aa 240 to 631) was also raised commercially (Imgenex, San Diego, Calif.). Both antibodies had very high titers, as determined by enzyme-linked immunosorbent assay. Both antibodies recognized the WT hRad21 protein as a specific 122-kDa band in Western blot analysis and effectively immunoprecipitated endogenous hRad21 from various human and rodent cell lines and tissue lysates. Immunodetection of the 122-kDa band was blocked competitively by pretreatment of the lysates with recombinant hRad21 protein or synthetic C-terminal peptides. Both antibodies were also effective in immunohistochemistry and immunofluorescence staining of both paraffin-embedded and tissue culture slides.

Antisera. The monoclonal antisera were obtained as follows: human poly-(ADP-ribose) polymerase (PARP) from PharMingen, San Diego, Calif.; Flag epitope and mouse β-actin from Sigma, St. Louis, Mo.; *c-myc* epitope (9E10), bacterial *trpE*, caspase-3, caspase-7, tubulin, and lamin from Oncogene Research Products, Cambridge, Mass. hRad21 N-terminal antibody was a gift from J.-M. Peters (Research Institute of Molecular Pathology, Vienna, Austria).

Cell cultures and transfection. MCF-7 breast carcinoma cells, human chorio-carcinoma JEG3 cells, and IMR90 primary lung fibroblast cells were obtained from the American Type Culture Collection (ATCC) and were maintained per ATCC protocol. Human Molt4 and Jurkat T-cell leukemia cells (both obtained from ATCC) were grown in RPMI 1640 medium supplemented with 10% fetal bovine serum and maintained at 37°C, 95% humidity, and an atmosphere of 5% CO$_2$. EL-12 mouse mammary epithelial cells were obtained from the Medina Laboratory (Baylor College of Medicine) and maintained as previously described (27). Cells were transfected with appropriate plasmids in 100-mm-diameter dishes using Superfect or Effectene reagents from Qiagen (Valencia, Calif.) according to the manufacturer's protocol. A fixed amount of plasmid DNA was used in any given experiment. The total amount of expression vector DNA was equalized by the addition of blank vectors to control for promoter competition effects. When necessary, transfection efficiency was monitored by use of 1 μg of pDsRedi-Mito plasmid (Clontech, Palo Alto, Calif.) per transfection. Transfection efficiency was determined by counting the percentage of red fluorescent cells in five random fields under a microscope with appropriate fluorescent channels.

Drug treatments. Etoposide (VP-16) (20-mg/ml injections) and camptothecin were purchased from GensiaSicor Pharmaceuticals (Irvine, Calif.) and Sigma, respectively. Camptothecin was dissolved in dimethyl sulfoxide (DMSO) and stored in aliquots at −20°C. Cells were plated at a concentration of 6 × 10^6 cells/ml and treated with appropriate concentrations of drugs. Molt4 cells were treated with etoposide, while Jurkat cells were treated with camptothecin for 8 h unless otherwise indicated. Controls were treated with equivalent dosages of vehicle. The caspase inhibitor z-VAD-FMK was also dissolved in DMSO and stored at −20°C. Peptide aldehydes MG115 and MG132 were obtained from Peptide Institute, Inc. (Lexington, Ky.) and dissolved at a concentration of 10 mM in DMSO. Cells were treated with a 0.025 mM concentration of proteasome inhibitors for 8 h before harvesting. 15-Deoxy-delta(12,14)-prostaglandin J$_2$ (15dPGJ$_2$) was purchased from Cayman Chemical Co. (Ann Arbor, Mich.). Induction of apoptosis in JEG3 cells by using 15dPGJ$_2$ was carried out as previously described (19).

Protein analysis and IP. Cells were pelleted by low-speed centrifugations (800 × g for 5 min) and lysed in RIPA buffer (phosphate-buffered saline [PBS], 1% Nonidet P-40, 0.1% sodium dodecyl sulfate [SDS], 0.5% sodium deoxycholate) or PBSTDS buffer (PBS, 1% Triton X-100, 0.1% SDS, 0.5% sodium deoxycholate) containing protease and phosphatase inhibitors (1 mM EDTA, 0.2 mM phenylmethylsulfonyl fluoride, 1 μg of pepstatin per ml, 30 μl of aprotinin per ml, 0.5 μg of leupeptin per ml, 100 mM sodium orthovanadate, 100 mM sodium fluoride) (all from Sigma) for 10 to 15 min on ice, followed by passage through a 21-gauge needle. When appropriate, additional phosphatase inhibitor cocktails I and II (Sigma) were added to the lysis buffer at a dilution of 1:100. Lysates were then centrifuged at 1,000 × g for 20 min, and the supernatants were aliquoted and frozen at −80°C until use. Protein samples were also made from the cytoplasmic and nuclear fractions of apoptosis-induced Molt4 cells by using protocols previously described (5). The purities of the cytosolic and nuclear fractions were verified by Western blotting with antibodies to tubulin and nuclear lamin, respectively. After protein quantification (using detergent-compatible protein dye and bovine serum albumin from Bio-Rad as standards) and normalization, 10 to 40 μg of protein extracts was electrophoresed on SDS-polyacrylamide gel electrophoresis (PAGE) gels and transferred to polyvinylidene difluoride (PVDF) membranes (Millipore, Bedford, Mass.). The filters were initially blocked with 5% nonfat dry milk in Tris-buffered saline containing 0.1% Tween 20 for 1 to 2 h at room temperature and then probed with hRad21 mAb or hRad21 pAb at a 1:1,000 dilution, 1.5 μg of *myc* epitope/ml, 2.5 μg of Flag epitope/ml, β-actin at a 1:100,000 dilution, or PARP antiserum at a 1:2,000 dilution. The bound antibodies were visualized by the enhanced chemiluminescence detection system (Amersham, Buckinghamshire, England), in combination with the horseradish peroxidase-conjugated anti-mouse or anti-rabbit secondary antibodies as appropriate, and the intensity of the specific bands in the exposed films was quantified. In some of the later experiments, bound primary antibodies were detected with IRD800 dye-labeled, appropriate species-specific secondary antisera and the signal was visualized on a Li-Cor (Lincoln, Nebr.) Odyssey infrared scanner. Immunoprecipitation (IP) was performed as follows. A 1.0-ml sample of cell lysate was precleared by incubation with 10 μl of normal mouse immunoglobulin G (IgG) and 20 μl of protein G plus agarose (Oncogene Research Products) at 4°C for 1 h on a rotator. The precleared lysate was collected after centrifugation at 800 × g for 15 min. A 0.5- to 1.0-ml sample of precleared lysate normalized for protein concentrations was incubated at 4°C for 1 h with primary antibodies followed by the addition of 20 μl of protein A and protein G plus agarose. The mix was then incubated at 4°C for another 12 to 16 h on a rotator. Precipitates were then washed four times with 1 ml of ice-cold PBS, with a final wash in the lysis buffer before electrophoresis and Western blot analysis.

Mapping of hRad21 apoptotic cleavage sites. Apoptosis was induced in Molt4 T cells by treatment with 10 μM etoposide for 8 h. Protein lysates were subjected to IP using hRad21 mAb or a control bacterial *trpE* mAb. The immunoprecipitated samples were run on SDS-6% PAGE gels that included 0.1 mM sodium thioglycolate (Sigma) as a scavenger in the upper running buffer. Electrophoresed samples were then electroblotted onto PVDF membranes at 400 mA for 45 min at room temperature (~25°C) using CAPS [3-(cyclohexylamino)propane-sulfonic acid] buffer (10 mM CAPS, 10% methanol, pH 11). At the end of the transfer, the blotted membranes were rinsed with water for 2 to 5 min, stained with 0.05% Coomassie blue in 1% acetic acid–50% methanol for 5 to 7 min, destained in 50% methanol until the background was pale blue (5 to 15 min), and finally rinsed with water for 5 to 10 min. Appropriate bands were cut out and air dried and sent to the protein chemistry core laboratory at Baylor College of Medicine for N-terminal sequencing.

Immunocytochemistry and detection of apoptosis. EL-12 cells were grown on Falcon culture slides. Medium was poured off before the cells were treated with UV (0, 50, 100, or 200 J/m^2). Fresh medium was added immediately after UV radiation. Cells were fixed with cold methanol after 6 h of UV treatment unless otherwise noted. Double staining of hRad21 was performed by incubating anti-hRad21 mAb and rabbit anti-C-terminal-hRad21 pAb. The signals of mAb and pAb were visualized by the addition of rhodamine-labeled goat anti-mouse IgG (1:100) and fluorescein-labeled goat anti-rabbit IgG (1:800) (Molecular Probes), respectively. Slides were mounted with Vectashield mounting medium with DAPI (4′,6′-diamidino-2-phenylindole; H-1200, Vector) and sealed with nail makeup. Images were obtained with a Zeiss inverted fluorescence microscope coupled to an Axiocam high-resolution digital camera operated with Axiovision 3.0 software (Carl Zeiss Inc., Thornwood, N.Y.).

For detection of apoptosis in transiently transfected 293T and MCF-7 cells, 1 million cells were seeded onto 100-mm-diameter culture dishes 2 days prior to transfection. Cells were transfected with the indicated hRad21 constructs when they reached 60% confluence. For DAPI staining, cells were cotransfected with 5 μg of pDsRed1-Mito (Clontech) and 5 μg of pCS2MT, pCS2MT Rad21 wild

type, pCS2MT Rad21 N terminus, or pCS2MT Rad21 C terminus by using the calcium phosphate method. At 16, 24, and 48 h posttransfection, cells were detached with trypsin and collected by centrifugation at 1,000 × g for 5 min. The samples were fixed with 4% paraformaldehyde in PBS (pH 7.2), mounted with Vectashield mounting medium with DAPI (H-1200, Vector), and examined by fluorescence microscopy. The intact and degraded nuclei of cells coexpressing pDsRed1 (with red fluorescence) were counted. About 50 fluorescent nuclei from each treatment group were screened and counted for normal morphology (rounded chromatin) or for apoptotic nuclei (fragmented and condensed chromatin). Data were expressed as the percentage of apoptotic cells among total counted cells. Each treatment was replicated three times. For Annexin V and TUNEL (terminal deoxynucleotidyltransferase-mediated dUTP-biotin nick end labeling) staining, 293T cells were transfected with 10 μg of pCS2MT, pCS2MT Rad21 wild type, pCS2MT Rad21 N-terminus, or pCS2MT Rad21 C-terminus by using the calcium phosphate method. After 16, 24, and 48 h, the cells were detached and collected as described above. Annexin V (Annexin V-FITC [fluorescein isothiocyanate] apoptosis direction kit) and TUNEL staining (MEB-STAIN apoptosis kit direct) were performed according to the manufacturer's protocol (MBL, Watertown, Mass.). Staining of the cells with Annexin V-FITC and propidium iodide (PI) was used to distinguish between cells undergoing apoptosis (PI negative) and those that were necrotic or dead (PI positive). Apoptotic cells were identified with TUNEL staining using fluorescein-dUTP as the substrate.

The caspase-3 activities in Molt4 cells were measured using a caspase-3 assay kit from Clontech according to the manufacturer's protocol.

Proteolytic cleavage assay of the in vitro transcribed and translated hRad21. ^{35}S-hRad21 or unlabeled (nonisotopic) hRad21 was produced by in vitro transcription-translation using the TNT rabbit reticulocyte lysate system (Promega, Madison, Wis.). Rabbit reticulocyte lysate was combined with 1 μg of plasmid DNA containing either the WT hRAD21 cDNA (pCS2MT-hRAD21) or one of the hRAD21 ACS mutants, ACS-mut-I or ACS-mut-II, and SP6 RNA polymerase. Reaction in the absence of plasmid DNA served as a negative control. Reaction mixtures were incubated at 30°C for 90 min. In vitro cleavage reaction was performed as previously described (9). In brief, 6 μl of in vitro translated ^{35}S-hRad21 (WT), ACS-mut-I, or ACS-mut-II was combined with 30 μl of reaction buffer (20 mM HEPES, pH 7.4, 2 mM dithiothreitol, 10% glycerol) and one of the following enzyme sources: 2 μl (200 U) of recombinant caspase-3, 2 μl (4 U) of caspase-7, or 2 μl (10 μg) of Molt4 cell lysates (treated with DMSO or 10 μM etoposide for 6 h). The cleavage reaction was performed at 37°C for 1 h, after which 8 μl of 6× sample buffer with dithiothreitol was added to stop the reaction. Twenty microliters of this reaction was electrophoresed on SDS-6% PAGE gels, fixed with methanol and acetic acid for 30 min, dried on a gel dryer, and exposed to a Storm imager. Bands were quantified using Image-Quant 5.2 software (Molecular Dynamics, Inc., Sunnyvale, Calif.). Unlabeled (nonisotopic) hRad21 from the TNT reactions was also incubated as described above in the presence or absence of caspase-3 or caspase-7. Samples were then analyzed by SDS-PAGE followed by Western blotting with hRad21 antiserum.

Data analysis. The differences between the apoptosis levels in cells transfected with various hRad21 constructs were measured using a paired test of proportions based on binomials (8). The results of the caspase-3 activity assay were analyzed using Student's t test.

RESULTS

We report the role of hRad21 in the apoptotic response and cleavage of hRad21 protein in human cells by a caspase-like activity.

Cleavage of hRad21 during apoptosis. While examining the expression of Rad21 in mammalian cells after DNA damage, we surprisingly identified the cleavage of hRad21 protein after induction of apoptosis. hRad21 was cleaved during etoposide-induced apoptosis in human Molt4 T-cell leukemia cells. Induction of apoptosis resulted in the generation of approximately 64- and 60-kDa cleavage products, as determined with an hRad21 mAb (Fig. 1). The cleavage of hRad21 in Molt4 cells was a function of etoposide dosage (Fig. 1A), as the ratio of cleaved hRad21 to full-length protein appeared to be directly proportional to increasing doses of etoposide over the tested range (10 to 50 μM). hRad21 cleavage products were
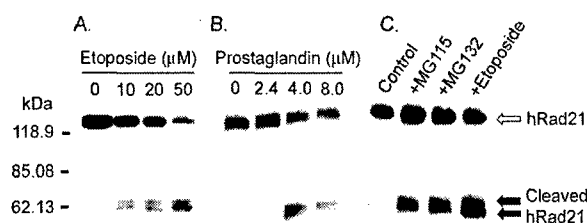

FIG. 1. Apoptosis-induced cleavage of hRad21 in Molt4 T-cell leukemia and JEG3 choriocarcinoma cells treated with etoposide, prostaglandin, and proteasome inhibitors. (A) Dose-related cleavage of hRad21 in Molt4 T-cell leukemia cells treated with increasing concentrations of etoposide (10 to 50 μM) for 6 h. (B) JEG3 cells treated with 15DPGJ$_2$ (2.4 to 8 μM) for 16 h. (C) Molt4 cells were also treated with a 0.025 mM concentration of proteasome inhibitors, MG115, and MG132 for 8 h. Lysates of these samples were resolved on an SDS-PAGE (4 to 20% acrylamide) gel, transferred to a nitrocellulose membrane, and analyzed by Western blot using a monoclonal hRad21 antibody. Induction of apoptosis resulted in the generation of approximately 64- and 60-kDa hRad21 cleavage products (shown by the closed arrows). Full-length hRad21 (122 kDa) is indicated by the open arrow.

also detected in a number of other cell lines following induction of apoptosis by DNA-damaging agents (ionizing radiation and topoisomerase inhibitors) (data not shown) and/or non-DNA-damaging agents (prostaglandin [Fig. 1B], proteasome inhibitor [Fig. 1C], cycloheximide treatment, and cytokine withdrawal [data not shown]). In addition, equivalent doses of ionizing radiation in cells that are resistant to apoptosis (Raji lymphoid leukemia and H1299 large-cell lung carcinoma cells) did not generate this band (data not shown); thus, it was not a simple by-product of DNA damage.

Translocation of the carboxy-terminal hRad21 fragment to the cytoplasm after induction of apoptosis. Molt4 cells were treated with 10 μM etoposide for 0, 1, 2, 3, 4, 6, and 12 h. Induction of apoptosis was verified by determination of caspase-3 activity (Fig. 2A), Annexin V staining (Fig. 2F), the cleavage of PARP, and the morphology of DAPI-stained nuclei (data not shown). Western blot analysis of cytoplasmic and nuclear fractions by using a C-terminal hRad21 antibody detected a 122-kDa protein band in the noninduced cells (0 h), and as reported before (12), full-length hRad21 was found exclusively in the nuclear fractions (Fig. 2B). However, induction of apoptosis resulted in the early (4 h after induction) generation of approximately 64- and 60-kDa cleavage products, as determined by a C-terminal hRad21 antibody (Fig. 2B). As indicated by Annexin V staining, hRad21 cleavage shows a clear temporal relationship with the early events of apoptosis when the cell membrane remains intact. Annexin V is a calcium-dependent, phospholipid binding protein with high affinity for phosphatidylserine (PS) and can be used to identify apoptotic cells with exposed PS. As PS exists in the inner face of the cell membrane in normal cells, Annexin V cannot bind to the cell membrane. Early in apoptosis, however, PS is translocated from the inner to the outer surface of the cell membrane. As Annexin V has high affinity for PS, it can then bind to the cell surface via interaction with PS. In the late stages of apoptosis, Annexin V continues to bind PS, and as the membrane permeability is increased, PI can enter the cell and bind DNA. In addition to our results with Annexin V staining,
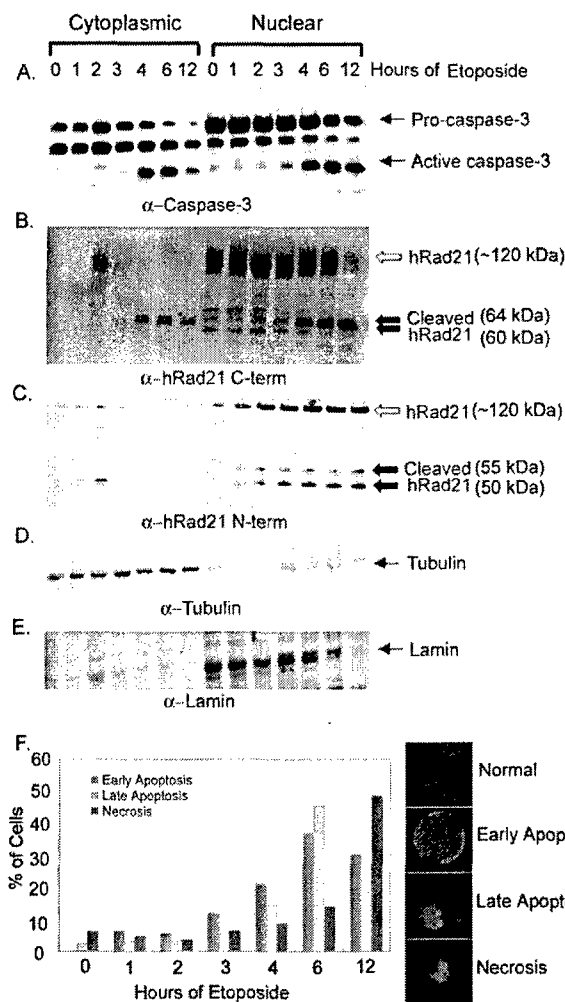
FIG. 2. Time course of etoposide-induced hRad21 cleavage. Molt4 cells were incubated in the absence (0 h) or presence of 10 μM etoposide for 1, 2, 3, 4, 6, and 12 h. At the end of the incubation period, lysates from cytoplasmic and nuclear fractions were made. (A) Induction of apoptosis was verified by determination of caspase-3 activity in a Western blot analysis using anti-caspase-3 mAb. Pro-caspase-3 and active caspase-3 are indicated. (B and C) The time course of cleavage of hRad21 protein in etoposide-induced cytoplasmic and nuclear fractions was examined using C-terminal (B) and N-terminal (C) Rad21 pAbs. Full-length hRad21 (122 kDa; open arrow) and C-terminal cleaved 60- and 64-kDa fragments and N-terminal 50- and 55-kDa fragments (closed arrows) are indicated. (D and E) The purities of the cytoplasmic (D) and nuclear (E) fractions were verified with antibodies to tubulin and nuclear lamin, respectively. (F) Quantitative measurement of Annexin V staining showing early and late events of apoptosis. Cells stained with Annexin V (green fluorescence in the outer cell membrane) represent early stages of apoptosis, while cells with both PI-stained nuclei (red fluorescence) and Annexin V staining (green fluorescence in the outer cell membrane) represent late stages of apoptosis. Cells with PI-stained red fluorescence represent necrotic cells only. Normal cells lack any staining. Examples from each category are shown at right. Values represent the percentage of green (early stage of apoptosis), green plus red (late stage of apoptosis), or red (necrotic) fluorescent cells, with 120 cells being used at each time point.
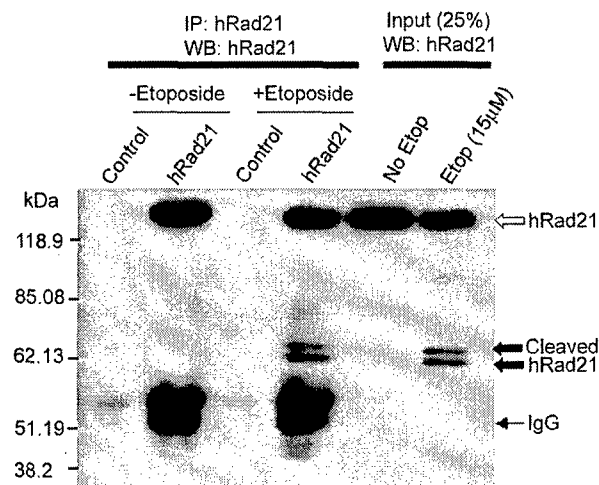

FIG. 3. IP and Western blot (WB) analyses of the hRad21 cleavage products. Apoptosis was induced in Molt4 T cells by treatment with 10 μM etoposide (Etop) for 8 h. Protein lysates were subjected to IP using hRad21 mAb or a control bacterial *trpE* mAb. Both monoclonal and polyclonal C-terminal antibodies detected 64- and 60-kDa bands (closed arrows), indicating that these bands are from the C-terminal portion of the cleaved protein.

we found that the progressive increase in the cleavage of hRad21 correlates with the level of active caspase-3 (Fig. 2A).

Although hRad21 is a nuclear protein, the cleaved products are found in both nuclear and cytoplasmic fractions after induction of apoptosis (Fig. 2B). The identities of these two cleavage products were investigated using an N-terminal hRad21 antibody. As expected, the N-terminal antibody could not detect the 64- and 60-kDa cleavage products either in the cytoplasmic or nuclear fraction. In contrast, this antibody detected two other bands (approximately 50 and 55 kDa) only in the nuclear fractions (Fig. 2C). The purities of the cytosolic and nuclear fractions were verified with antibodies to tubulin and lamin, respectively (Fig. 2D and E). These results indicate that hRad21 may potentially be cleaved at two different sites following induction of apoptosis. The C-terminal hRad21 cleavage products but not the N-terminal hRad21 products are found in the cytoplasm after cleavage following induction of apoptosis.

The identities of the cleavage products were confirmed through recognition by mAbs to hRad21 in IP and Western blot analyses (Fig. 3). hRad21 mAb selectively immunoprecipitated both the 60- and 64-kDa hRad21 cleavage products, along with the native 122-kDa full-length hRad21 protein in etoposide-induced Molt4 cells. Analysis of cells treated with vehicle only and control IP with isotype bacterial TrpE antibody did not detect these bands, confirming that the cleaved bands were hRad21 products. Both monoclonal and polyclonal C-terminal antibodies detected the 64- and 60-kDa bands, confirming that these bands were derived from the C-terminal portion of the cleaved protein.

Translocation of hRad21 was further investigated in EL-12 mammary epithelial cells by immunofluorescence staining using the monoclonal and C-terminal hRad21 polyclonal antisera. Unlike Molt4 cells, EL-12 cells have a large cytoplasm to facilitate visualization. In these cells, Rad21 was entirely nu-
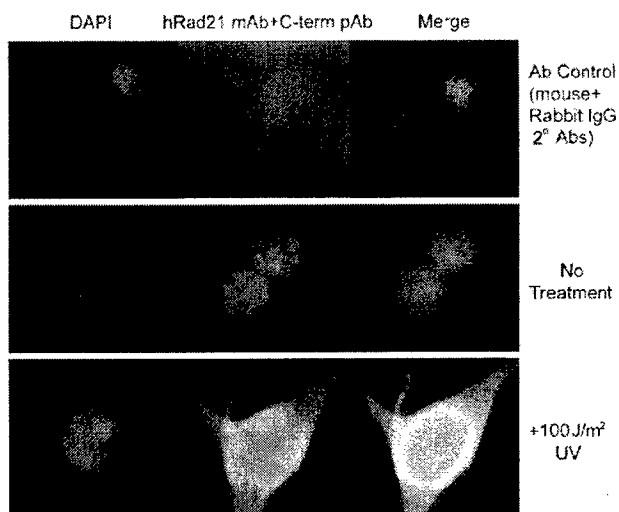
FIG. 4. C-terminal Rad21 cleavage product translocates to the cytoplasm after induction of apoptosis. Apoptosis was induced by treatment of EL-12 mammary epithelial cells with UV light (100 J/m²). UV-treated (bottom panel) and untreated control (middle panel) cells were subjected to immunofluorescence staining and microscopy using a C-terminal hRad21 pAb (green fluorescence) and hRad21 mAb (red fluorescence), respectively. The signals of mAb and pAb were visualized by the addition of rhodamine-labeled goat anti-mouse IgG and fluorescein-labeled goat anti-rabbit IgG, respectively. The upper panel shows the background staining (negative control) from the fluorescein-labeled secondary antibody in the presence of normal mouse and rabbit IgGs. The nuclear material is visualized by DAPI staining (blue fluorescence). Panels at right show merged images of red, blue, and green fluorescence.

FIG. 5. Caspase peptide inhibitors inhibit etoposide-induced cleavage of hRad21. Molt4 cells were treated with 20 μM z-VAD-FMK, a broad-spectrum caspase inhibitor, 1 h prior to etoposide (10 μM) treatment for 6 h. At the end of the incubation period, protein lysates were analyzed on an SDS–6% PAGE gel followed by Western blot analysis using hRad21 C-terminal pAb.

clear (Fig. 4, middle panel). Apoptosis was induced by treatment of EL-12 cells with UV light (100 J/m²) and was verified by the cleavage of Rad21 and PARP (data not shown). Immunofluorescence staining of the UV-treated cells by the C-terminal antibody clearly demonstrated translocation of the cleaved C-terminal Rad21 to the cytoplasm (Fig. 4, bottom panel).

Inhibition of hRad21 cleavage by caspase peptide inhibitors. Peptide-based caspase inhibitors inhibited the apoptosis-induced cleavage of hRad21, suggesting the involvement of caspases in hRad21 cleavage (Fig. 5). Molt4 cells were treated with 20 μM z-VAD-FMK, a broad-spectrum caspase inhibitor, 1 h prior to etoposide (10 μM) treatment. As shown in Fig. 5, treatment with z-VAD-FMK completely blocked etoposide-induced hRad21 cleavage. In an in vitro cleavage assay (described below), z-VAD-FMK also inhibited caspase-3-induced cleavage of ³⁵S-hRad21 (data not shown).

Identification of the apoptotic cleavage site in hRad21. The hRad21 cleavage site was mapped through N-terminal sequencing of the immunoprecipitated hRad21 cleavage products from electroblotted and Coomassie-stained PVDF membranes (Fig. 6). Sequencing of the 64-kDa band revealed that hRad21 was cleaved at Asp-279 (D^{279}). The N-terminal sequence of the 64-kDa band was SVDPVEP. In the full-length protein, the sequence immediately N terminal to the D^{279} cleavage site was PDSPD²⁷⁹. Thus, there was a repeat of the PDS sequence encompassing the cleavage site, i.e., PDSPD²⁷⁹/ SVDPVEP (Fig. 6A). We were not successful in sequencing
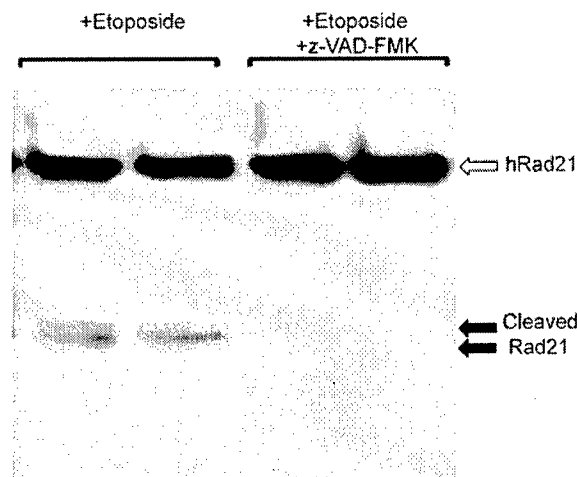
the 60-kDa band, possibly because of an N-terminal blocking effect. To verify whether specific cleavage occurred at D^{279} in hRad21 after induction of apoptosis, we introduced a point mutation (mut-I) by substituting an alanine (A) for aspartate (D) at this position of hRad21 (D279A) (Fig. 6B). Furthermore, because of the repetition of the cleavage sequence ²⁷⁵PDSPDS²⁸⁰, we made a second mutant construct (mut-II) by substituting alanine (A) for both aspartate (D) and serine (S) residues, i.e., hRad21 (²⁷⁵PDSPDS²⁸⁰ to ²⁷⁵PAAPAA²⁸⁰). We then transiently transfected Molt4 cells with WT or mutant hRad21 constructs tagged with the myc epitope at the N terminus and treated these cells with etoposide as indicated. As shown in Fig. 6C, antibody against myc tag (9E10) revealed the proteins encoded by the transfected hRad21 WT and hRad21 ACS-mut-I and ACS-mut-II constructs. However, the cleavage fragments were detected only for WT hRad21, not for either of the mutants, indicating that a point mutation at D^{279} prevented cleavage (Fig. 6C). We reprobed the blot with anti-hRad21 mAb and found that both the 60- and 64-kDa C-terminal fragments were present in all etoposide-treated cells (data not shown), confirming that endogenous hRad21 was cleaved in cells transfected with hRad21 mutants.

Involvement of caspases in hRad21 cleavage. Closer inspection of the adjoining sequence at the Rad21 apoptotic cleavage site (DSPD²⁷⁹) (Fig. 6A) revealed a putative recognition sequence for a primitive caspase, Ced3. This sequence is conserved Rad21 in vertebrates, including humans, mice, and frogs (*Xenopus* spp.). The sequence of the putative cleavage site, together with the inhibitory effect of a panel of caspase inhibitors on etoposide-induced apoptosis in Molt4 cells, indicated the possible involvement of a caspase family protease. While the experiments with caspase inhibitors suggested the involvement of a caspase family of protease(s) in the pathway leading to hRad21 cleavage, they did not demonstrate direct internal cleavage of hRad21 by a caspase. We therefore utilized an in vitro cleavage assay as described previously for the retinoblas-

A.

HumanRad21	267	----------DENVS.SPDSPDS.PVEPMPTMTTQTTI.HEE.FAL.PI.KE---T.AR.RKLI.SVKE
MouseRad21	267	----------DNGS.PDSPDS.PVEPMPTMTTQTTI.HEE.FAL.PI.KE---T.AR.RKLI.SVKE
Xenopus Rad21	265	----------DNVS.APDSPDS.PVEELPTMTTQTTI.HEE.FAI.PI.KE---T.AR.RKLI.SVKE
Arabidopsis Rad21	259	TLNEKEPTI.SIEEK.SG.RHSAPELRS.SPGSAAGCE.EPADFVHPS.QLV.DE.PP.Q---PG.A.RINPDGVT
Drosophila Rad21	266	VPSPATSLVNSIE.EKEENNLNGHAS.SENVPMQN----EITL.ME.E.FAI.PI.YKGV-T.AR.RKLI.EIKN
C.elegans Rad21	264	HP----------VPEHA.TVQNDDG.FDYQPFEPENVEPSRP.SPR.FAL.PI.EHMEGRKK.QS.ARKLI.AETM
Fission Yeast Rad21	251	L.DLG-------LDPN.GDQ.GAHAPATE.EQAETSSIL.PSDIM.DIS.R.SAAG.EG.QVVESATAQ.QEKINFQK
Budding Yeast Rad21	216	W.DLG-------ITEKD.QHNDI.DN.EQGRRLGEI.SRE.PTI.F.ELDIEKEAA.G-------N.DTITDAM
consensus	321	d mg vd v ne e falepidity k kr rklivd

B.
Wild Type

```
ATG GGT GGG CCT GAT AGT CCT GAT TCA GTG GAT
 M   G   G   P   D   S   P   D   S   V   D
                            ↑
```

ACS Mutant-I   279

```
ATG GGT GGG CCT GAT AGT CCT GCT TCA GTG GAT
 M   G   G   P   D   S   P   A   S   V   D
```

ACS Mutant-II

```
ATG GGT GGG CCT GCT GCT CCT GCT GCA GTG GAT
 M   G   G   P   A   A   P   A   A   V   D
```
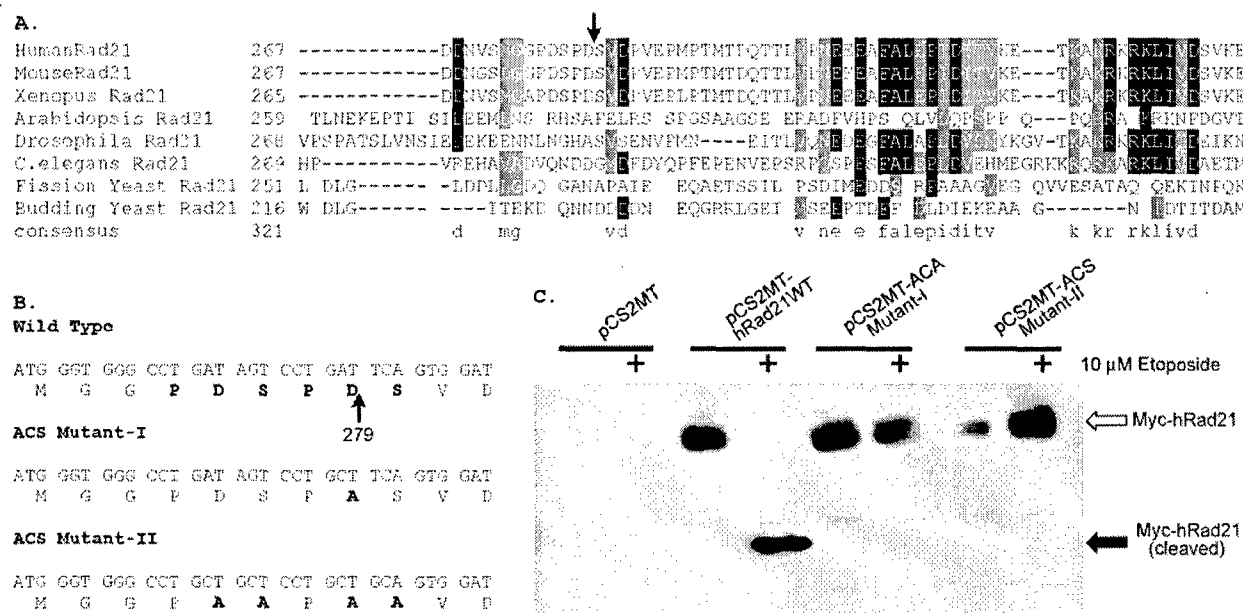
C.

FIG. 6. Characterization of the apoptotic cleavage site of hRad21. The hRad21 cleavage site was mapped biochemically, as described in Materials and Methods, through N-terminal sequencing of a Coomassie-stained PVDF membrane that was electroblotted with immunoprecipitated hRad21 cleavage products. (A) Comparison of the apoptotic cleavage recognition site and the adjoining sequence of hRad21 with those of other vertebrates (MouseRad21 and Xenopus Rad21) and simpler eukaryotes. C.elegans, *Caenorhabditis elegans*. The arrow indicates the peptide bond cleaved during apoptosis. (B) Construction of the apoptotic cleavage site mutants, ACS-mut-I and ACS-mut-II, to verify whether specific cleavage occurs at D^{279} in hRad21 after induction of apoptosis, by introduction of a point mutation to substitute an alanine (A) for aspartate (D) (mut-I) or alanine (A) for aspartate (D) and serine (S) (mut-II). (C) Molt4 cells were transiently transfected with blank vector (pCS2MT), WT hRad21 (pCS2MT-*hRAD21*), or ACS mutants tagged with *myc* epitope at their N termini (pCS2MT-ACSmut-I or pCS2MT-ACSmut-II) and treated with etoposide as indicated. Lysates were analyzed with SDS–6% PAGE followed by Western blot analysis using antibody against *myc* tag (9E10) to distinguish the cleavage products from the native forms of transfected hRad21 WT and hRad21 ACS-mut-I and ACS-mut-II proteins.

toma protein (9) to examine the ability of purified caspase to cleave hRad21 (Fig. 7). We used two caspases, caspase-3 and caspase-7, that are major regulators of apoptosis in diverse cell types (35) (Fig. 7A), along with lysates from Molt4 cells treated with etoposide (apoptotic lysate) or vehicle (nonapoptotic lysate), to examine their role in hRad21 cleavage (Fig. 7B). Together, caspase-3 and caspase-7 comprise the caspase-3 subfamily, and both enzymes recognize and cleave after the consensus cleavage site DXXD (E. S. Alnemri, D. J. Livingston, D. W. Nicholson, G. Salvesen, N. A. Thornberry, W. W. Wong, and J. Yuan, Letter, Cell **87**:171, 1996). Addition of recombinant caspase-3 or caspase-7 to the in vitro transcribed and translated hRad21 in rabbit reticulocyte lysates clearly resulted in the production of a 64-kDa hRad21 fragment (Fig. 7A and B). The 64-kDa fragment produced by these caspases precisely comigrated with the 64-kDa band produced by apoptotic Molt4 lysates, while the control (nonapoptotic) cell lysate could not cleave hRad21 protein. On the other hand, both of the hRad21 ACS mutants failed to be cleaved by these two caspases or by apoptotic cell lysates in this assay, strongly suggesting that caspase-3- or caspase-7-like enzymes in the apoptotic cells or extracts were responsible for cleavage at the putative caspase recognition site (D^{279}) of hRad21.

In addition to the 64-kDa fragment, several other fragments were generated by caspase-3 and -7. It is possible that the 64-kDa fragment was degraded further by these caspases, re-
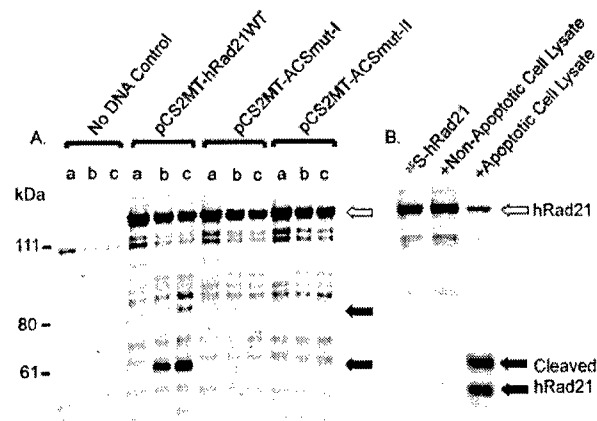

FIG. 7. Cleavage of in vitro translated hRad21 by recombinant caspase-3 and caspase-7. (A) In a cleavage reaction, in vitro translated unlabeled (nonisotopic) WT hRad21 or ACS mutant hRad21 (ACS-mut-I or ACSMut-II) in the rabbit reticulocyte lysate were incubated with saline (vehicle) (lanes a), caspase-3 (lanes b), or caspase-7 (lanes c). TNT reactions in the absence of plasmid DNA served as a negative control. Samples were analyzed on an SDS–6% PAGE gel followed by Western blotting with hRad21 C-terminal pAb. Molecular weight markers are shown at left. (B) ^{35}S-hRad21 was incubated in the absence of extract (left lane) or in the presence of Molt4 cell lysates treated with DMSO (middle lane) or 10 μM etoposide (right lane) for 6 h. Samples were resolved on a 4 to 20% gradient SDS-PAGE gel, fixed with methanol and acetic acid for 30 min, dried on a gel dryer, and exposed to a Storm imager.
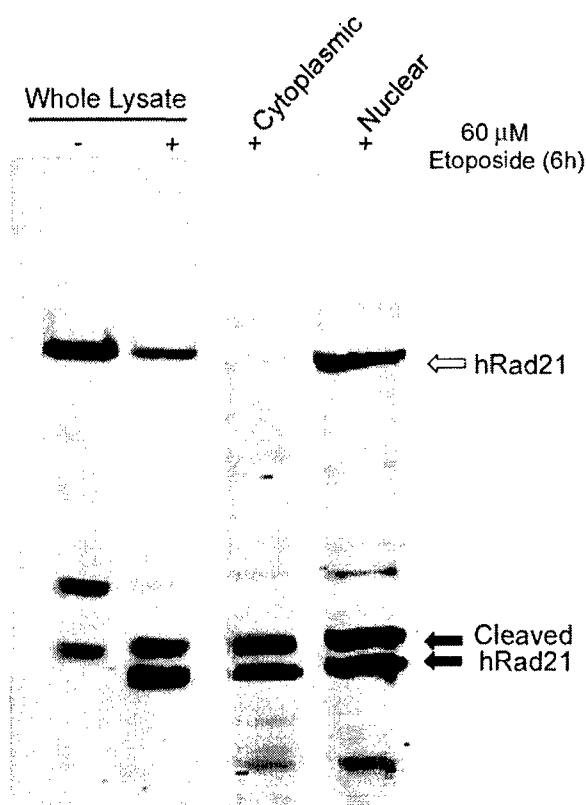
FIG. 8. Cleavage of hRad21 in caspase-3-deficient MCF-7 breast cancer cells. Apoptosis was induced by treatment of MCF-7 cells with 60 μM etoposide for 6 h. Cells treated with DMSO (vehicle) served as a control. Whole-cell lysates or lysates from the cytoplasmic and nuclear fractions were electrophoresed on an SDS–6% PAGE gel and subjected to Western blot analysis using hRad21 mAb. Arrows indicate the hRad21 products.

sulting in the production of smaller fragments. In the presence of caspase-7 but not caspase-3, a 95-kDa fragment of hRad21 was also generated, suggesting another caspase site N-terminal to the D^{279} cleavage site. In the in vitro cleavage assay, caspase-3 and -7 failed to generate the 60-kDa hRad21 fragment that accompanies the 64-kDa fragment after induction of apoptosis, suggesting that the cleavage site generating the 60-kDa fragment was not recognized by caspase-3 and -7.

To determine whether caspase-3 is essential for the in vivo cleavage of hRad21, we utilized a caspase-3-deficient MCF-7 breast cancer cell line (21). In experiments using etoposide- or tamoxifen-induced apoptosis in MCF-7 cells, hRad21 cleavage products were detected, indicating that caspase-3 was not essential for hRad21 cleavage (Fig. 8) and that a caspase other than caspase-3 can act upon hRad21 to cause cleavage following induction of apoptosis.

hRad21 C-terminal cleavage product promotes apoptosis. A possible role for hRad21 in the induction of apoptosis was first seen in preliminary experiments in which overexpression of hRad21 in Molt4, 293T, and MCF7 cells resulted in apoptotic phenotypes. However, conclusive evidence for the role of cleaved hRad21 in the promotion of apoptosis was obtained by transient transfection of 293T and Molt4 cells with cytomega-

lovirus (CMV) promoter-driven *myc*-tagged mammalian expression plasmids encoding the full-length hRad21 or cDNAs encoding the two cleavage products, hRad21 N-terminal (aa 1 to 279) or hRad21 C-terminal (aa 280 to 631) proteins (Fig. 9 and 10). Analysis of transfected 293T cells by multiple apoptosis assays, including examination of cellular morphology under light microscopy (Fig. 9A) and staining with TUNEL (Fig. 9B), Annexin V (Fig. 9C), and DAPI (Fig. 9D), clearly indicated the ability of the 64-kDa C-terminal hRad21 to induce apoptosis. Quantitative analysis of 293T cells transfected with C-terminal hRad21 plasmids indicated a significant increase ($P < 0.05$) of nuclear degradation in cells transfected with the C-terminal hRad21 compared with that in cells transfected with vector control (pCS2MT), WT hRad21 (pCS2MT Rad21), or N-terminal hRad21 (pCS2MT hRad21 N-term) (Fig. 10A). In these cells, apoptosis was also assayed by monitoring the phenotype of the DAPI-stained nuclei. As shown in Fig. 9D, cells transfected with hRad21 C-terminal plasmid displayed significantly more ($P < 0.05$) cellular and nuclear phenotypes typical of apoptosis, such as a round shape with shrunken cell volume, chromatin condensation, and nuclear disintegration, compared with the vector control and cells expressing the full-length and N-terminal hRad21 constructs. Similar results were also obtained with MCF7 and Molt4 cells (data not shown).

The proapoptotic activity of the C-terminal hRad21 was further strengthened by a significantly increased level ($P < 0.05$) of caspase-3 activity in Molt4 cells transfected with hRad21 C-terminal plasmids compared with that in cells transfected with the WT hRad21 (pCS2MT hRad21) and N-terminal hRad21 (pCS2MT hRad21 N-term) constructs. As shown in Fig. 10B, C-terminal hRad21 overexpression resulted in a five- to sevenfold increase in caspase-3 activity compared with that of the empty vector control. Although overexpression of WT hRad21 induced moderate but statistically insignificant levels of apoptosis, as determined by caspase-3 activity in Molt4 cells, overexpression of the hRad21 C-terminal cleavage product but not the N-terminal hRad21 cleavage product dramatically increased caspase-3 activity ($P < 0.05$) in Molt4 cells (Fig. 10B). The transfection efficiency in Molt4 cells was 35%, as determined by cotransfection with a red fluorescence plasmid, pDSRed1-mito. Similar results for caspase-3 activity were also obtained with MCF-7 and 293T cells transfected with hRad21 constructs (data not shown).

Further experiments using vectors to direct hRad21 expression either to the cytoplasm or nucleus demonstrated that expression of hRad21 in the cytoplasm but not in the nucleus resulted in the cleavage of hRad21 protein and induction of apoptosis, as determined by assaying of caspase-3 activity (Fig. 11). It is interesting that both the *myc*-tagged (cytoplasmic) hRad21 and the WT (normally nuclear) hRad21 were cleaved in the cells transiently transfected with the pCMV/*myc*/cyto-hRad21 construct (Fig. 11). In summary, the C-terminal hRad21 cleavage product was proapoptotic, as determined by increased caspase-3 activity and apoptotic morphology, and its translocation to the cytoplasm may play a role in promoting apoptosis. These findings demonstrate the ability of the 64-kDa Rad21 fragment to induce apoptosis.

Apoptotic cleavage of hRad21 is not affected by the status of the p53 tumor suppressor protein in the cell. In view of the pivotal role of the p53 gene product in regulation of the cell

Vector Control   Rad21 WT   Rad21 N-term   Rad21 C-term

A. Bright Field

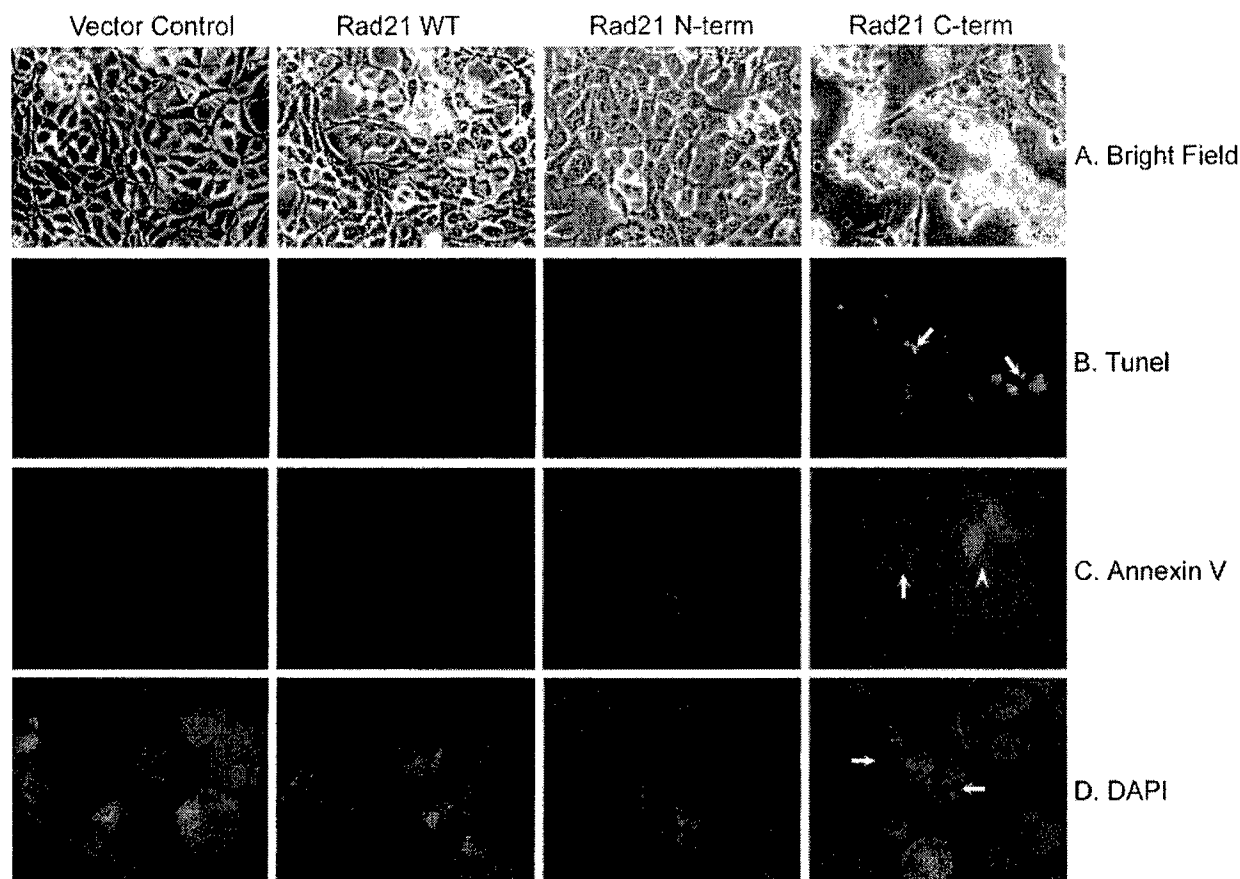B. Tunel

C. Annexin V

D. DAPI

FIG. 9. Analysis of the proapoptotic activity of C-terminal hRad21 in 293T cells by examination of cellular morphology (A) and staining with TUNEL (B), Annexin V (C), and DAPI (D). In panels A to C, 293T cells were transiently transfected with CMV promoter-driven *myc*-tagged mammalian expression plasmids (pCS2MT) encoding the full-length hRad21 or cDNAs encoding the two cleavage products, hRad21 N-terminal (aa 1 to 279) and hRad21 C-terminal (aa 280 to 631) proteins. In panel D, in addition to the above constructs, cells were also cotransfected with a red fluorescence plasmid (pDsRed1-Mito) to account for the hRad21-transfected cells. Note that C-terminal-hRad21-transfected cells have round morphology, as shown in light micrographs (A) and are positive for TUNEL (B) and Annexin V (C) staining (arrows). PI was used to detect the integrity of cell membranes in Annexin V-FITC staining; hence, the nuclei of some apoptotic cells were red (arrowhead). In panel D, more than 50% of the C-terminal-hRad21-transfected cells with red fluorescence have fragmented nuclei and condensed chromatin, typical of apoptotic cells.

cycle and apoptosis, we examined the role of p53 in the apoptotic cleavage of hRad21. We used two myeloid leukemia cell lines, ML-1 and HL-60, with WT and null p53 genotypes, respectively (32, 41). Apoptosis was induced using UV (20 J/m^2) and ionizing radiation (20 Gy) in these cells. As shown in Fig. 12, the induction of apoptosis resulted in the cleavage of hRad21 protein in both cell lines, indicating the lack of a role for p53 in hRad21 cleavage.

DISCUSSION

Sister chromatid cohesion during DNA replication plays a pivotal role in accurate chromosomal segregation in the eukaryotic cell cycle. Rad21 is one of the major cohesin subunits that keeps sister chromatids together until anaphase when proteolytic cleavage by separase allows the chromosomes to separate. Mitotic cleavage sites in Rad21 in yeast as well as in humans have been mapped (12, 37, 39). Here we show that hRad21 cleavage occurs during apoptosis and is induced by

various agents, including DNA-damaging (ionizing radiation and topoisomerase inhibitors) and non-DNA-damaging agents (cycloheximide treatment, cytokine withdrawal, and treatment with proteasome inhibitors). We have biochemically mapped the apoptotic cleavage site in human Rad21 (PDSPD^{279}/S), which is distinct from the mitotic cleavage sites (DRE-IMR^{172}/E and IEEPSR^{450}/L) previously described (12). The apoptotic cleavage site is conserved among vertebrate species, and it is likely that cleavage is mediated by a nuclear caspase or caspase-like molecule, as this cleavage site bears the characteristic caspase-3 subfamily recognition motif (DXXD) and hRad21 is cleaved in vitro by the two major apoptosis executioner caspases, caspase-3 and caspase-7. hRad21 cleavage is not restricted to transformed cancer cells, as induction of apoptosis resulted in hRad21 cleavage in the primary cell line IMR90 (data not shown) as well as the nontransformed immortal cell line EL-12.

Cleavage of hRad21 appears to be an early event in the apoptotic pathway. The immunofluorescence experiments and
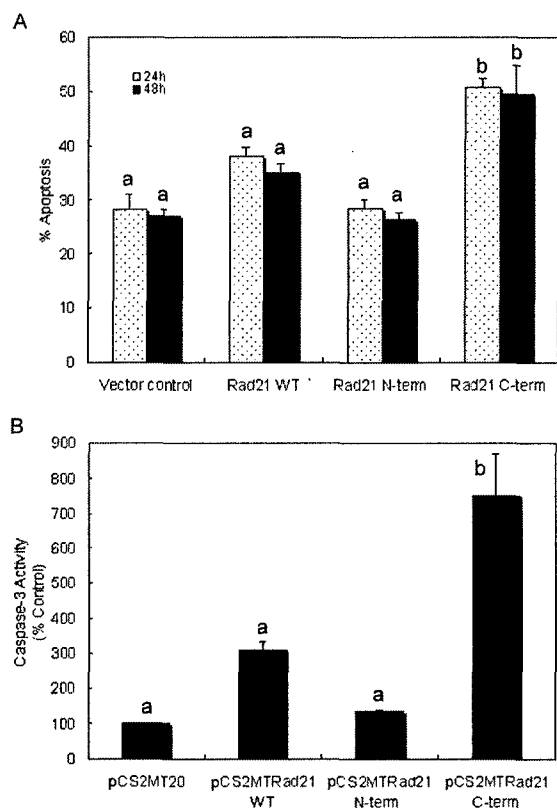
A

B

FIG. 10. Quantitative analysis of the proapoptotic activity of C-terminal hRad21 in 293T and Molt4 T-cell leukemia cells. Cells were transiently transfected with CMV promoter-driven *myc*-tagged mammalian expression plasmids encoding the full-length hRad21 or cDNAs encoding the two cleavage products, hRad21 N-terminal (aa 1 to 279) and hRad21 C-terminal (aa 280 to 631) proteins. 293T cells were also cotransfected with the red fluorescence plasmid pDSRed1-mito to account for the hRad21-transfected cells. Nuclear degradation of 293T cells (A) and caspase-3 activity in Molt4 cells (B) were measured as described in Materials and Methods. For the nuclear degradation assay, cells were collected and fixed 24 and 48 h after transfection. The samples were stained with DAPI and examined with fluorescence microscopy. Cells with fragmented nuclei or condensed chromatin were counted as apoptotic. For each sample, a total of 50 intact and degraded nuclei of cells coexpressing pDsRed1-mito (with red fluorescence) was counted. Each data point represents the average and standard errors of the mean from three experiments. The data for caspase-3 activity shown in panel B are the averages and standard errors of the mean from two experiments. The results of the apoptosis assay were analyzed using a binomial test of proportions and those for caspase-3 activity were analyzed using Student's t test. Data labeled "a" are significantly different ($P < 0.05$) from data labeled "b."

Western blot analysis of nuclear and cytoplasmic fractions of cells undergoing apoptosis demonstrate the translocation of the hRad21 C-terminal cleavage products to the cytoplasm early (3 to 4 h after insult) in apoptosis. Our results clearly show that hRad21 proteolysis by a caspase family protease at D^{279}/S leads to the production of a proapoptotic C-terminal cleavage product. The specific protease that cleaves hRad21 in vivo and promotes hRad21-induced apoptosis is yet to be identified. Nuclear changes determined by Annexin V staining and examination of the morphology of DAPI-stained nuclei indicate a strong temporal relationship between hRad21 cleavage
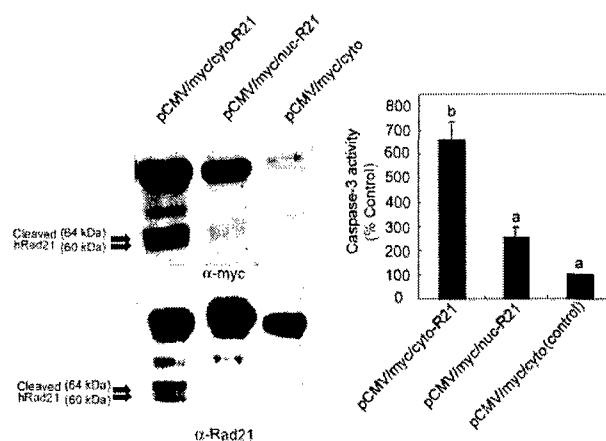

FIG. 11. Effect of the cytoplasmic expression of hRad21 on apoptosis and cleavage of hRad21 protein. Molt4 cells were transiently transfected with the constructs pCMV/*myc*/cyto-hRad21 and pCMV/*myc*/nuc-hRad21, which direct the expression of the recombinant protein to the cytoplasm and nucleus, respectively. Empty PCMV/*myc*/cyto vector served as a control. At 48 h posttransfection, protein lysates were made and subjected to Western blot analysis using c-*myc* epitope (9E10) and hRad21 mAb to detect the fusion and/or native hRad21 proteins, respectively. Lysates were also used for the assaying of caspase-3 activity as described in Materials and Methods. The data for caspase-3 activity shown at right are the averages and standard errors of the mean from two experiments. Individual values were compared using Student's t test, and values labeled "a" are significantly different ($P < 0.05$) from that labeled "b."

and apoptosis. As determined by Annexin V staining, hRad21 cleavage correlates well with the early events of apoptosis when the cell membrane remains intact. Furthermore, the progressive increase in the cleavage of hRad21 correlates well with the level of caspase activation, as determined by assaying of by caspase-3 activity. Translocation of the 64-kDa hRad21 cleavage product to the cytoplasm early in apoptosis may act as a nuclear signal that promotes and accelerates subsequent events of apoptosis. The specificity of this product was determined further, as the N-terminal hRad21 cleavage product neither translocates nor has the ability to induce apoptosis. We have not explored the role of the 60-kDa hRad21 product generated at a cleavage site other than D^{279}/S in the apoptotic process.

The physiological significance of cohesin hRad21 cleavage in apoptosis is intriguing. The nuclear signal(s) that detects subsequent events of apoptosis in the cytoplasm and mitochondria has remained elusive. It is possible that cleavage of hRad21 at the onset of apoptosis and the translocation of the C-terminal cleavage product to the cytoplasm act as cues to accelerate the apoptotic process. Supporting evidence in favor of this possibility include the following: (i) hRad21 is not normally cytoplasmic; (ii) early in apoptosis, hRad21 is found in the cytoplasm; and (iii) directed expression of either the C-terminal or full-length hRad21 to the cytoplasm induces apoptosis. It is not clear whether localization of C-terminal hRad21 to the cytoplasm is due to an active or a passive transport process following cleavage. The carboxy-terminal fragment contains a putative nucleolar localization signal sequence, which argues against a passive transport process. These findings further strengthen the notion that the translocation of the C-terminal
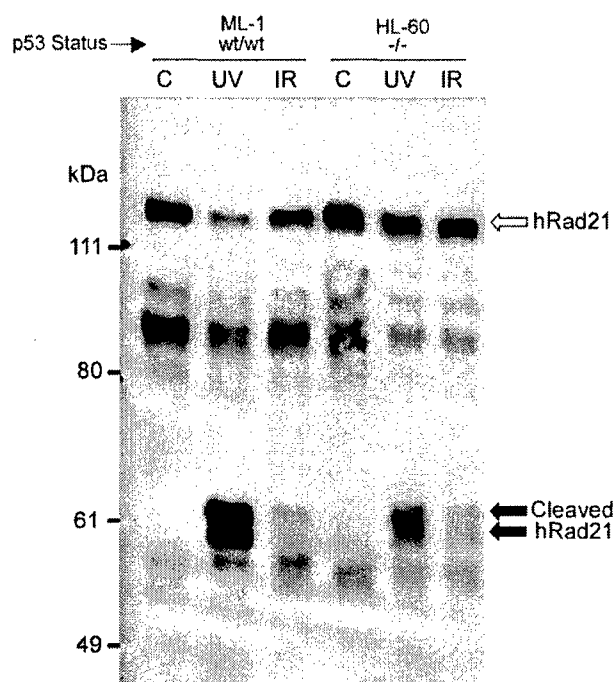
FIG. 12. Effect of p53 status on the cleavage of hRad21. Apoptosis was induced in the myeloid leukemia cell lines ML-1 and HL-60, with WT and null p53 genotypes, respectively, by treatment of the cells with UV light (20 J/m^2) or ionizing radiation (IR) (20 Gy). Six hours after treatment, protein lysates were made and resolved by SDS–6% PAGE followed by Western blot analysis using hRad21 mAb. Arrows indicate hRad21 cleavage products. C, control without UV or IR treatment.

hRad21 protein to the cytoplasm may play a functional role in apoptosis.

We have firmly established the proapoptotic activity of the C-terminal hRad21 cleavage product by several apoptotic assays, including Annexin V staining, TUNEL methods, quantitative measurement of DAPI-stained nuclear morphology, and assaying of caspase-3 activity. However, the exact mechanism by which cleaved hRad21 induces apoptosis requires further investigation. It is interesting that a BLAST search of the apoptosis database (www.apoptosis-db.org) indicated that C-terminal hRad21 possesses a stretch of 80 aa (aa 282 to 362) that has homology to the tumor necrosis factor receptor superfamily and other apoptosis-inducing proteins, including TRAIL-R2 and death receptor 5. However, the functional significance of this domain in apoptosis-inducing proteins is not known.

The caspase-mediated proteolysis of hRad21 and the partial removal of hRad21 from the nucleus may also expose the chromosomal DNA to DNase and other proteins responsible for chromatin condensation and apoptotic DNA fragmentation. hRad21 was originally isolated in fission yeast as an essential protein with a role in the repair of DNA double-strand breaks induced by ionizing radiation (2). It is therefore logical to think that disruption of the DNA repair function of hRad21 may be necessary during the execution of apoptosis. This notion has been strengthened by recent findings that a number of DNA repair enzymes such as Rad51 (15), ATM (13), DNA-PK (4), and PARP (22) and cell cycle regulators such as retino-

blastoma protein (9) are cleaved by caspases. Coordinated destruction of the DNA repair machinery and cell cycle regulators by the caspase family of proteases therefore constitutes a physiologically relevant process that promotes and accelerates chromosomal condensation and DNA fragmentation without interference by the cell cycle and DNA repair machinery. Unlike hRad21, however, cleavage products of these other DNA repair proteins have not been reported to play a direct role in promoting apoptosis. In this case, cleavage of hRad21 by caspases may play a unique role in amplifying the apoptotic signal by elevating the level of caspase activity. A similar mechanism for amplifying the apoptotic signal for the caspase substrate vimentin has recently been described (3).

The p53 tumor suppressor protein plays a central role in the regulation of the cell cycle and apoptosis after DNA damage (17, 34). In the event that DNA damage is more severe and not repairable, p53 directs the cells into apoptosis through the Bax/Bcl-2 pathway. p53 status does not appear to have any effect on the apoptotic cleavage of hRad21 after DNA damage (i.e., UV and ionizing radiation), indicating the lack of involvement of the p53 pathway in hRad21 cleavage. It is possible that a parallel p53-independent pathway may regulate the genotoxic-damage-induced cleavage of hRad21.

Finally, it is interesting that cleavage of cohesin hRad21 is carried out by a separase in mitosis and by a caspase in apoptosis at different sites in the protein. Both of these proteases belong to the distantly related CD clan protease family (38), suggesting an evolutionarily conserved mechanism shared by the mitotic and apoptotic machinery. hRad21 may serve as the link between the two key cellular processes of mitosis and apoptosis. In summary, in contrast to the previously described functions of Rad21, i.e., in chromosome segregation and DNA repair, cleavage of the cohesion protein and translocation of the C-terminal cleavage product to the cytoplasm are early events in the apoptotic pathway that amplify the apoptotic signal in a positive-feedback manner, possibly by activating more caspases. These results provide the framework for identification of the physiologic role of hRad21 in the apoptotic response in normal and malignant cells.

ADDENDUM IN PROOF

A similar conclusion regarding the function of RAD21 in apoptosis has been published by F. Chen et al. (J. Biol. Chem **277:**16775–16781, 2002).

REFERENCES

1. **Biggins, S., and A. W. Murray.** 1999. Sister chromatid cohesion in mitosis. Curr. Opin. Genet. Dev. **9:**230–236.
2. **Birkenbihl, R. P., and S. Subramani.** 1992. Cloning and characterization of

rad21, an essential gene of *Schizosaccharomyces pombe* involved in DNA double-strand-break repair. Nucleic Acids Res. **20:**6605–6611.

3. Byun, Y., F. Chen, R. Chang, M. Trivedi, K. J. Green, and V. L. Cryns. 2001. Caspase cleavage of vimentin disrupts intermediate filaments and promotes apoptosis. Cell Death Differ. **8:**443–450.

4. Casciola-Rosen, L. A., G. J. Anhalt, and A. Rosen. 1995. DNA-dependent protein kinase is one of a subset of autoantigens specifically cleaved early during apoptosis. J. Exp. Med. **182:**1625–1634.

5. Chaturvedi, M. M., R. LaPushin, and B. B. Aggarwal. 1994. Tumor necrosis factor and lymphotoxin. Qualitative and quantitative differences in the mediation of early and late cellular response. J. Biol. Chem. **269:**14575–14583.

6. Ciosk, R., W. Zachariae, C. Michaelis, A. Shevchenko, M. Mann, and K. Nasmyth. 1998. An ESP1/PDS1 complex regulates loss of sister chromatid cohesion at the metaphase to anaphase transition in yeast. Cell **93:**1067–1076.

7. Cohen-Fix, O., J.-M. Peters, M. W. Kirschner, and D. Koshland. 1996. Anaphase initiation in *Saccharomyces cerevisiae* is controlled by the APC-dependent degradation of the anaphase inhibitor Pds1p. Genes Dev. **10:**3081–3093.

8. Downie, N. M., and R. W. Heath. 1965. Basic statistical methods, 2nd ed. Harper & Row, New York, N.Y.

9. Fattman, C. L., S. M. Delach, Q. P. Dou, and D. E. Johnson. 2001. Sequential two-step cleavage of retinoblastoma protein by caspase-3/-7 during etoposide-induced apoptosis. Oncogene **20:**2918–2926.

10. Funabiki, H., H. Yamano, K. Kumada, K. Nagao, T. Hunt, and M. Yanagida. 1996. Cut2 proteolysis required for sister-chromatid separation in fission yeast. Nature **381:**438–441.

11. Guacci, V., D. Koshland, and A. Strunnikov. 1997. A direct link between sister chromatid cohesion and chromosome condensation revealed through the analysis of MCD1 in *S. cerevisiae*. Cell **91:**47–57.

12. Hauf, S., I. C. Waizenegger, and J.-M. Peters. 2001. Cohesin cleavage by separase required for anaphase and cytokinesis in human cells. Science **293:**1320–1323.

13. Hotti, A., K. Jarvinen, P. Siivola, and E. Holtta. 2000. Caspases and mitochondria in c-Myc-induced apoptosis: identification of ATM as a new target of caspases. Oncogene **19:**2354–2362.

14. Huang, D. C. S., L. A. O'Reilly, A. Strasser, and S. Cory. 1997. The anti-apoptosis function of Bcl-2 can be genetically separated from its inhibitory effect on cell cycle entry. EMBO J. **16:**4628–4638.

15. Huang, Y., S. Nakada, T. Ishiko, T. Utsugisawa, R. Datta, S. Kharbanda, K. Yoshida, R. V. Talanian, R. Weichselbaum, D. Kufe, and Z. M. Yuan. 1999. Role for caspase-mediated cleavage of Rad51 in induction of apoptosis by DNA damage. Mol. Cell. Biol. **19:**2986–2997.

16. Hunter, T. 1997. Oncoprotein network. Cell **88:**333–346.

17. Israels, L. G., and E. D. Israels. 1999. Apoptosis. Stem Cells **17:**306–313.

18. Jallepalli, P. V., I. C. Waizenegger, F. Bunz, S. Langer, M. R. Speicher, J.-M. Peters, K. W. Kinzler, B. Vogelstein, and C. Lengauer. 2001. Securin is required for chromosomal stability in human cells. Cell **105:**445–457.

19. Keelan, J. A., T. A. Sato, K. W. Marvin, J. Lander, R. S. Gilmour, and M. D. Mitchell. 1999. 15-Deoxy-delta(12,14)-prostaglandin J₂, a ligand for peroxisome proliferator-activated receptor-gamma, induces apoptosis in JEG3 choriocarcinoma cells. Biochem. Biophys. Res. Commun. **262:**579–585.

20. Koshland, D. E., and V. Guacci. 2000. Sister chromatid cohesion: the beginning of a long and beautiful relationship. Curr. Opin. Cell Biol. **12:**297–301.

21. Kurokawa, H., K. Nishio, H. Fukumoto, A. Tomonari, T. Suzuki, and N. Saijo. 1999. Alteration of caspase-3 (CPP32/Yama/apopain) in wild-type MCF-7 breast cancer cells. Oncol. Rep. **6:**33–37.

22. Lazebnik, Y. A., S. H. Kaufmann, S. Desnoyers, G. G. Poirier, and W. C.

Earnshaw. 1994. Cleavage of poly (ADP-ribose) polymerase by a proteinase with properties like ICE. Nature **371:**346–347.

23. Leismann, O., A. Herzig, S. Heidmann, and C. F. Lehner. 2000. Degradation of *Drosophila* PIM regulates sister chromatid separation during mitosis. Genes Dev. **14:**2192–2205.

24. Levine, A. J. 1997. p53, the cellular gatekeeper for growth and division. Cell **88:**323–331.

25. Lipponen, P., S. Aaltomaa, V.-M. Kosma, and K. Syrjanen. 1994. Apoptosis in breast cancer as related to histopathological characteristics and prognosis. Eur. J. Cancer **30A:**2068–2073.

26. Losada, A., and T. Hirano. 2001. Shaping the metaphase chromosome: coordination of cohesion and condensation. Bioessays **23:**924–935.

27. Medina, D., and F. S. Kittrell. 1993. Immortalization phenotype dissociated from the preneoplastic phenotype in mouse mammary epithelial outgrowths in vivo. Carcinogenesis **14:**25–28.

28. Michaelis, C., R. Ciosk, and K. Nasmyth. 1997. Cohesins: chromosomal proteins that prevent premature separation of sister chromatids. Cell **91:**35–45.

29. Minn, A. J., L. H. Boise, and C. B. Thompson. 1996. Expression of Bcl-X_L and loss of p53 can cooperate to overcome a cell cycle checkpoint induced by mitotic spindle damage. Genes Dev. **10:**2621–2631.

30. Nasmyth, K., J.-M. Peters, and F. Uhlmann. 2000. Splitting the chromosome: cutting the ties that bind sister chromatids. Science **288:**1379–1385.

31. Nasmyth, K. 2001. Disseminating the genome: joining, resolving, and separating sister chromatids during mitosis and meiosis. Annu. Rev. Genet. **35:**673–745.

32. O'Connor, P. M., J. Jackman, I. Bae, T. G. Myers, S. Fan, M. Mutoh, D. A. Scudiero, A. Monks, E. A. Sausville, J. N. Weinstein, S. Friend, A. J. Fornace, Jr., and K. W. Kohn. 1997. Characterization of the p53 tumor suppressor pathway in cell lines of the National Cancer Institute anticancer drug screen and correlations with the growth-inhibitory potency of 123 anticancer agents. Cancer Res. **57:**4285–4300.

33. Shimada, A. 1996. PCR-based site-directed mutagenesis. Methods Mol. Biol. **57:**157–165.

34. Strasser, A., L. O'Connor, and V. M. Dixit. 2000. Apoptosis signaling. Annu. Rev. Biochem. **69:**217–245.

35. Thornberry, N. A., and Y. Lazebnik. 1998. Caspases: enemies within. Science **281:**1312–1316.

36. Uhlmann, F., and K. Nasmyth. 1998. Cohesion between sister chromatids must be established during DNA replication. Curr. Biol. **8:**1095–1101.

37. Uhlmann, F., F. Lottspeich, and K. Nasmyth. 1999. Sister chromatid separation at anaphase onset is promoted by cleavage of the cohesin subunit Scc1. Nature **400:**37–42.

38. Uhlmann, F., D. Wernic, M. A. Poupart, E. V. Koonin, and K. Nasmyth. 2000. Cleavage of cohesin by the CD clan protease separin triggers anaphase in yeast. Cell **103:**375–386.

39. Waizenegger, I. C., S. Hauf, A. Meinke, and J.-M. Peters. 2000. Two distinct pathways remove mammalian cohesin from chromosome arms in prophase and from centromeres in anaphase. Cell **103:**399–410.

40. Warren, W. D., S. Steffensen, E. Lin, P. Coelho, M. Loupart, N. Cobbe, J. Y. Lee, M. J. McKay, T. Orr-Weaver, M. M. Heck, and C. E. Sunkel. 2000. The *Drosophila* RAD21 cohesin persists at the centromere region in mitosis. Curr. Biol. **10:**1463–1466.

41. Zhan, Q., S. Fan, I. Bae, C. Guillouf, D. A. Liebermann, P. M. O'Connor, and A. J. Fornace. 1994. Induction of *bax* by genotoxic stress in human cells correlates with normal p53 status and apoptosis. Oncogene **9:**3743–3751.

42. Zou, H., T. J. McGarry, T. Bernal, and M. W. Kirschner. 1999. Identification of a vertebrate sister-chromatid separation inhibitor involved in transformation and tumorigenesis. Science **285:**418–422.

Hormone-Induced Chromosomal Instability in p53-Null Mammary Epithelium

Debananda Pati,[1] Bassem R. Haddad,[3] Albert Haegele,[6] Henry Thompson,[6] Frances S. Kittrell,[2] Anne Shepard,[2] Cristina Montagna,[4] Nenggang Zhang,[1] Gouqing Ge,[1] Subhendu Kumar Otta,[1] Maureen McCarthy,[5] Robert L. Ullrich,[7] and Daniel Medina[2]

Departments of [1]Pediatrics, Hematology-Oncology, Texas Children's Cancer Center, and [2]Molecular and Cellular Biology, Baylor College of Medicine, Houston, Texas; [3]Lombardi Cancer Center and Institute for Molecular Human Genetics, Georgetown University Medical Center, Washington, District of Columbia; [4]Genetics Branch, Center for Cancer Research, NIH, Bethesda, Maryland; [5]Department of Microbiology, University of Texas Medical Branch, Galveston, Texas; [6]Division of Laboratory Research, AMC Cancer Research Center, Denver; [7]Department of Radiological Health Sciences, Colorado State University, Fort Collins, Colorado

ABSTRACT

The absence of p53 function increases risk for spontaneous tumorigenesis in the mammary gland. Hormonal stimulation enhances tumor risk in p53-null mammary epithelial cells as well as the incidence of aneuploidy. Aneuploidy appears in normal p53-null mammary epithelial cells within 5 weeks of hormone stimulation. Experiments reported herein assessed a possible mechanism of hormone-induced aneuploidy. Hormones increased DNA synthesis equally between wild-type (WT) and p53-null mammary epithelial cells. There were two distinct responses in p53-null cells to hormone exposure. First, Western blot analysis demonstrated that the levels of two proteins involved in regulating sister chromatid separation and the spindle checkpoint, Mad2 and separase (ESPL1) were increased in null compared with WT cells. In contrast, the levels of securin and Rad21 proteins were not increased in hormone-stimulated p53-null compared with WT cells. ESPL1 RNA was also increased in p53-null mouse mammary cells in vivo by 18 h of hormone stimulation and in human breast MCF7 cells in monolayer culture by 8 h of hormone stimulation. Furthermore, both promoters contained p53 and steroid hormone response elements. Mad2 protein was increased as a consequence of the absence of p53 function. The increase in Mad2 protein was observed also at the cellular level by immunohistochemistry. Second, hormones increased gene amplification in the distal arm of chromosome 2, as shown by comparative genomic hybridization. These results support the hypothesis that hormone stimulation acts to increase aneuploidy by several mechanisms. First, by increasing mitogenesis in the absence of the p53 checkpoint in G_2, hormones allow the accumulation of cells that have experienced chromosome missegregation. Second, the absolute rate of chromosome missegregation may be increased by alterations in the levels of two proteins, separase and Mad2, which are important for maintaining chromosomal segregation and the normal spindle checkpoint during mitosis.

INTRODUCTION

Genetic instability is a frequently reported event in p53 gene-deleted cells. The genetic instability observed in both normal and tumor cells of p53 knockout mice is evidenced by high incidences of aneuploidy (1, 2), centrosome amplification (2, 3), and loss of heterozygosity (4, 5). The frequency of these events is dependent on cell type and on specific cell stimuli. For example, inactivation of p53 in the diploid human colorectal cancer cell line HCT116 generates neither aneuploidy, chromosomal instabilities nor increased sister chromatid exchange (6). In a mouse transgenic model for choroid plexus tumors, absence of p53 does not generate chromosomal imbalances as measured by comparative genomic hybridization or flow cytometry (7). In the absence of p53, aneuploidy and centrosome amplification are common occurrences in cell cultures of fibroblasts

but infrequent in cell cultures of mammary epithelial cells (1, 8). However, a short-term exposure (5 weeks) to steroid hormones is sufficient to generate a high frequency of aneuploidy in these same mammary cells. Interestingly, centrosome amplification is not observed concomitantly with the aneuploidy (8).

Aneuploidy is a common characteristic of tumors (9–11) and has also been proposed as a necessary event for tumorigenesis (11, 12). Aneuploidy occurs not only in p53-null mouse mammary cells but also in estradiol-induced mammary tumors in the August Copenhagen Irish rat (13, 14). There is considerable controversy as to the importance of aneuploidy in tumorigenesis and tumor progression, although there is general agreement that it plays some role in the generation of the malignant phenotype (15, 16). The molecular mechanisms for generating aneuploidy are thought to be diverse, but all involve deregulation of some aspect of chromosomal replication and segregation (17). The mechanisms may be very specific, as in alterations of centrosome replication (18) and fidelity of the spindle apparatus, or in regulation of sister chromatid separation during mitosis (17). Additionally, the mechanisms may be passive, such as increased mitogenesis that leads to increased frequency of cells with missegregated chromosomes in the absence of normal cellular checkpoints (17, 19, 20). Finally, the mechanism might be nonspecific and generated as a result of random DNA damage. Estrogens are genotoxic in certain cell types, such as the rodent kidney cell (21, 22) and produce DNA adducts and mutations.

Both p53 heterozygous and p53-null mouse mammary epithelial cells are at increased risk for tumorigenesis (23, 24). The tumors are aneuploid and metastatic, and the pathogenesis mimics that observed in human breast cancer (25). The absence of p53 gene function does not significantly disturb normal mammary development, measured either morphologically (8, 26) or functionally (27). However, hormone stimulation of the gland increases not only tumorigenic risk but also the frequency of aneuploid cells (8). The mechanism of this hormone effect has not been established. In the experiments reported herein, we examine the possible cellular mechanisms for hormone-induced aneuploidy and conclude that the effect is both indirect because of increased mitogenesis and direct because of increased expression of two proteins involved in regulating chromosome segregation, separase (ESPL1) and Mad2.

MATERIALS AND METHODS

Transplantation

All of the mice were bred and maintained in a conventional mouse facility at Baylor College of Medicine with food and water provided ad libitum and the room temperature set at 70°F. The animal facility is American Association of Laboratory Animal Care accredited. Samples of mammary ducts were isolated from 7 8-week-old p53-null and p53 wild-type (WT) BALB/c mice and transplanted into the cleared mammary fat pads of 3-week-old WT BALB/c mice (23). The transplanted duct samples grew and filled the fat pads in 6–8 weeks. In each experiment, at least one fat pad was processed as a whole mount at 8 weeks to examine the growth and morphology of the outgrowth

---

(23). The remaining transplanted samples were examined as described below for the individual experiments.

In experiment 1, the proliferative and apoptotic indices of WT and p53-null normal mammary glands in the presence and absence of hormonal stimulation were examined using two different protocols. In both approaches, samples of the p53 WT normal duct and the p53-null normal duct were transplanted into the contralateral fat pads of each mouse. The first approach was a modification of an earlier experiment where the transplanted epithelium was subjected to a 5-week period of hormone stimulation starting two weeks after transplantation (8). In this modification, a silastic tubing containing estrogen (50 μg) plus progesterone (20 mg) was used instead of a pituitary isograft as in the original experiment. A pituitary isograft results in marked increases in the circulating levels of prolactin and progesterone (28). Five transplants were collected from the hormone-treated and untreated control mice for BrdUrd-labeling index. In the second approach, the mice were untreated until 8 weeks after transplantation, when the transplanted ducts had filled the mammary fat pad and were entering into a steady growth state. The animals were divided into three groups: untreated, received a silastic tubing containing estrogen (50 μg) and progesterone (20 mg), or untreated. Two-three transplants from each group were collected at 3 and 4 weeks thereafter and examined for morphological development, BrdUrd-labeling index, and apoptotic index.

Cell Culture

MCF-7 cells contain WT p53. The MCF-7 cells were seeded in improved minimal essential medium (IMEM) supplemented with 5 μg/ml bovine insulin and with 5% charcoal stripped serum for 24 h then in serum-free IMEM for another 48 h. Cells were exposed to hormones or left untreated in fresh serum-free media and harvested at 0, 0.5, 2, 8, 20, and 48 h posttreatment.

Immunohistochemistry

Samples of the transplants were evaluated for BrdUrd index by standard methods as described in Ref. 29. For BrdUrd immunohistochemistry, the samples were fixed in cold 4% paraformaldehyde for 1 h before being processed for paraffin-embedded sections. The antibody to BrdUrd was BD PharMingen BrdUrd *In Situ* Detection Kit (BD Biosciences, San Diego, CA). Animals were injected with BrdUrd (50 mg/kg body weight) 2 h before sacrifice. At least five separate samples were examined for each outgrowth line for each assay.

Apoptotic Index

Samples of transplant generations 7–8 were fixed in 10% neutral buffered formalin, embedded and stained with H&E, and evaluated for apoptotic indices by the terminal deoxynucleotidyl transferase-mediated nick end labeling method (30). For this assay, at least 3 samples were read per outgrowth and 500 cells counted per slide.

Genetic Analysis

Cytogenetic Analysis. Samples of the p53-null and p53 WT normal mammary cells, both untreated and hormone-stimulated, as well as p53-null primary tumors were evaluated for chromosome number and cytogenetic changes using conventional cytogenetic techniques as described in Ref. 8. For each preparation, 50 metaphases were counted. The types of cytogenetic changes examined included breaks, dicentrics, translocations, and aneuploidy.

Comparative Genomic Hybridization. Comparative genomic hybridization was performed on the hormone-stimulated mouse mammary epithelial cells of p53 WT and p53-null genotype. Each individual sample was composed of epithelial cell pellets isolated from three mammary fat pads. Comparative genomic hybridization was performed as described previously (31, 32). Normal control DNA was prepared from spleen tissue of normal mice, and test DNA was prepared from p53−/− and p53 +/+ mammary cells, using standard DNA extraction protocols. Test DNA was labeled with biotin-16-dUTP and control DNA with digoxigenin-11-dUTP (Boehringer Mannheim Corporation, Indianapolis, IN), using nick translation. Five hundred ng of each labeled genome (control DNA and test DNA) were hybridized in the presence of excess mouse Cot-1-DNA (Invitrogen, Carlsbad, CA), to metaphase chromosomes prepared from a karyotypically normal mouse. The biotin-labeled test genome was visualized with avidin conjugated to FITC (Vector Labora-

tories, Burlingame, CA), and the digoxigenin-labeled control DNA was visualized with a mouse antidigoxigenin antibody (Sigma, St. Louis, MO), followed by a goat antimouse antibody conjugated to tetramethylrhodamine isothiocyanate (Sigma). Chromosomes were counterstained with 4′,6-diamidino-2-phenylindole and embedded in antifading agent to reduce photobleaching. Gray scale images of the FITC-labeled test DNA, the tetramethylrhodamine isothiocyanate-labeled control DNA, and the 4′,6-diamidino-2-phenylindole counterstain for at least 15 metaphases/sample were captured with a cooled charge-coupled device camera (CH250; Photometrics, Tucson, AZ) connected to a Leica DMRBE microscope equipped with fluorochrome-specific optical filters TR1, TR2, and TR3 (Chroma Technology, Brattleboro, VT). Quantitative evaluation of the hybridization was performed using a commercially available comparative genomic hybridization analysis software (CW4000CGH). Average ratio profiles were computed as the mean value of at least 8 ratio images and were used to identify changes in chromosome copy number.

Western Blots

Western blot analysis of the effect of hormone stimulation on the expression of mitotic proteins involved in sister chromatid cohesion and separation was performed as described in Ref. 33. Briefly, after five weeks of hormone stimulation, the mammary glands containing transplants of both genotypes were collected, the epithelial cells were isolated and concentrated by gentle enzymatic treatment as described in Ref. 34, and the epithelial cell pellet processed for protein evaluation. The protein lysate was prepared as described previously (33). Cell pellets or tissue samples were lysed in radioimmunoprecipitation assay buffer (PBS, 1% NP40, 0.1% SDS, and 0.5% sodium deoxycholate) or PBS containing 1% Tritron X-100 (v/v), 0.5% (w/v) sodium deoxycholic acid, and 1% SDS (w/v) containing protease and phosphatase inhibitors (1 mM EDTA, 0.2 mM phenylmethylsulfonyl fluoride, 1 μg pepstatin/ml, 30 μl aprotinin/ml, 0.5 μg leupeptin/ml, 100 mM sodium orthovanadate, and 100 mM sodium fluoride; all from Sigma-Aldrich, St. Louis, MO) for 10–15 min on ice, followed by passage through a 21G needle. When appropriate, additional phosphatase inhibitors cocktail I and II (Sigma-Aldrich) were added to the lysis buffer at a dilution of 1:100. Lysates were then centrifuged at 1000 × g for 20 min, and the supernatants were aliquoted and frozen at −80°C until use. After protein quantification (using detergent compatible protein dye and BSA standards from Bio-Rad; Hercules, CA) and normalization, 30–40 μg of protein extracts were electrophoresed on SDS-PAGE gels and transferred to polyvinylidene difluoride membranes (Millipore, Bedford, MA). The filters were initially blocked with 5% nonfat-dry milk in Tris buffer saline containing 0.1% Tween 20 for 1–2 h at room temperature and then probed with hseparase mAb(1:500), p55CDC(1:500), Cdh1(1:500), mouse securin(1:250), hBub1(1:500), Mad2(1:500), hRad21(1:100), cyclin B1(1:500), Cdc2(1:1000), cyclin E(1:5000), Rad51(1:500), and β-actin antibodies(1:100,000). All of the antibodies except hRad21, hCdh1 (Neumarkers, Fremont, CA), and hseparase (a gift from Jan-Michael Peters, Research Institute of Molecular Pathology, Vienna, Austria) were purchased from Santa Cruz Biotechnology, Inc. (Santa Cruz, CA). The bound antibodies were visualized by the enhanced chemiluminescence detection system (Amersham, Buckinghamshire, England) in combination with the horseradish peroxidase-conjugated antimouse or antirabbit secondary antibodies as appropriate, and intensity of the specific bands in the exposed films was quantified. In some of the later studies, bound primary antibodies were detected with IRD800 dye-labeled appropriate species-specific secondary antisera, and signal was visualized on a Li-Cor Odyssey IR scanner (Lincoln, NE).

Northern Blots

Total RNA was isolated using RNeasy mini kit from Qiagen. Fifty micrograms of total RNA were diluted in ×2 RNA sampling buffer [20% formaldehyde; 1.65% Na$_2$HPO$_4$ (pH 6.8); 63.5% formamide; and 1× loading buffer] and separated on 1.0% agarose gel with 1 M formaldehyde in 1× running buffer [0.2 M 3-N-(morpholino) propanesulfonic acid, 50 mM sodium acetate, and 10 mM EDTA (pH 7.0)]. After transfer onto Nytran super charge membrane (Schleicher & Schuell), prehybridization, and hybridization in Clontech ExpressHyb solution at 75°C without/with [^{32}P]CTP-labeled *ESPL1* cDNA probe for 2 h, the membrane was washed 15 min twice with 1× washing buffer containing 300 mM NaCL, 30 mM sodium citrate, and 0.05% SDS at room
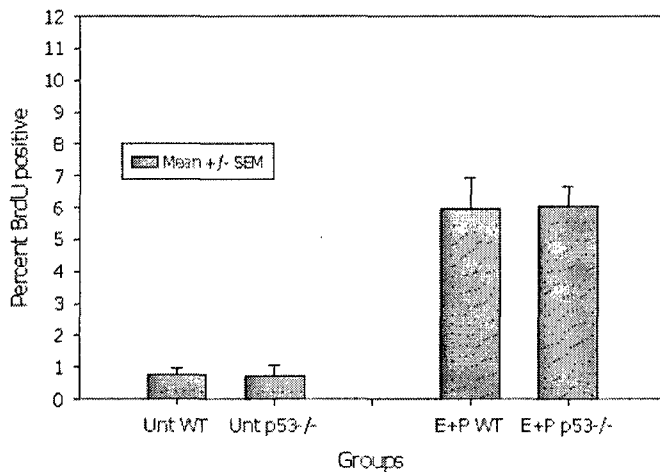
Fig. 1. Proliferation indices in p53-null and p53 WT normal epithelium exposed to estrogen (E) and progesterone (P) for 5 weeks. Mice received a silastic tubing of estrogen and progesterone at 2 weeks after transplantation. *Bars*, ±SEM; *n* = 5/group. (*Unt*, untreated).
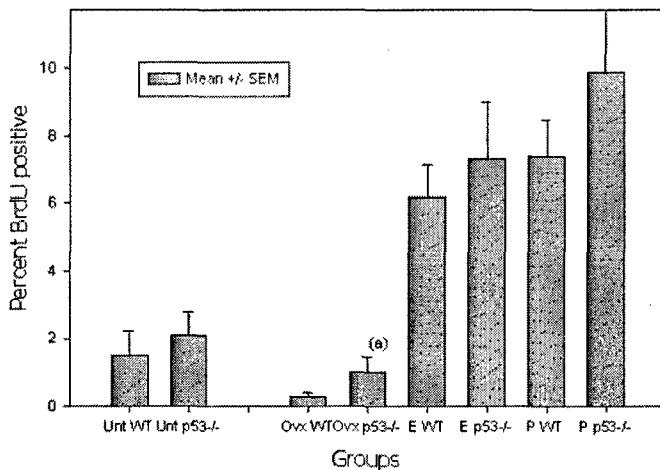

Fig. 2. Proliferation indices in p53-null and p53 WT normal epithelium exposed to estrogen (E) alone, progesterone (P) alone, or absence of estrogen and progesterone. Treatments were for 3–4 weeks starting at 8 weeks after transplantation. *Bars*, ±SEM; *n* = 5/group. (*a*, significantly different from WT; *OVX*, ovariectomized).

temperature followed by two washes with wash solution containing 15 mM NaCl, 1.5 mM sodium citrate, and 0.1% SDS at 50°C for 20 min each. Blots were visualized on a phosphor screen, and bands were quantitated on a STORM Imager (Molecular Dynamics). The membrane was then stripped (0.1× saline sodium citrate and 1% SDS) and rehybridized with keratin 18 or β-actin probes as a control. The absorbance of the bands was quantified using ImageQuant software, and the values were normalized relative to the control.

Promoter Analysis

The sequence of the 5' upstream region of both mouse and human *ESPL1* (separase) and Mad2 genes were extracted using the Ensembl database[8] and Stanford Source database[9] and analyzed for potential transcription start sites using Genomatix Suite and a neural network promoter prediction program. Potential transcriptional factor binding sites were analyzed using the Transcription Element Search Software and MatInspector/TRANSFAC programs (35).[10]

[8] Web address: www.ensembl.org.

[9] Web address: genome-www5.stanford.edu/cgi-bin/SMD/source/.

[10] See the following Web sites: http://genome.ucsc.edu/, http://www.ensembl.org, http://www.genomatix.de/, http://www.cbil.upenn.edu/tess/index.html, http://www.cbrc.jp/research/db/TFSEARCH.html, and http://www.fruitfly.org/seq_tools/promoter.html.

RESULTS

Effect of Hormones on Cell Proliferation. It is well established that both estrogen and progesterone induce cell proliferation in the normal mammary gland although to different extents and in different cell compartments. Therefore, the induction of aneuploidy in the p53-null cells by only low doses of progesterone was unexpected (8). We examined the effects of estrogen and/or progesterone on cell proliferation as a function of time of exposure. Examination of the whole mounts indicated that the two cell genotypes responded in a similar manner to the hormones. In the untreated mice, the mammary cells were organized as well-spaced primary and secondary ducts. The absence of hormones (ovariectomy) resulted in ducts with very narrow lumina, thus giving the appearance of atrophic ducts. The effect of estrogen was to increase slightly ductal density and to increase the size of the duct lumina. The effect of progesterone was distinct from estrogen because it led to an increase in small duct branching but only occasional alveolar buds. Estrogen and progesterone together resulted in development of alveoli.

The proliferation results are shown in Figs. 1 and 2. Three results are of interest. First, it is evident that the p53-null cells had a similar proliferative activity as the p53 WT cells at 7 weeks (Fig. 1) and at 11–12 weeks (Fig. 2) posttransplantation. The former time period represents cells approaching a steady state (80% fat pad filled) and the latter time period a maintained steady state with respect to proliferation. All of the three hormone treatments increased the proliferative activities of both the WT and null cells. The absolute percentage increases were the same for the WT and null cell phenotypes and were 4.1- and 3.5-fold, respectively, in estrogen-treated cells (Fig. 2), 4.9- and 4.7-fold, respectively, in progesterone-treated cells (Fig. 2), and 7.8- and 8.3-fold, respectively, in estrogen-progesterone treated cells (Fig. 1). Thus, there was little evidence of increased susceptibility of the null cells to hormone-induced regulation of proliferation. The deletion of hormones reduced the proliferative activities of the WT and null cells by 81% and 52%, respectively, at 4 weeks after ovariectomy (Fig. 2), confirming earlier experiments that the null cells, like WT cells, were ovarian hormone-dependent. The slightly higher proliferative activity of null cells in ovariectomized mice is statistically significant ($P < 0.05$) and probably has some significance over the lifetime of the mouse, because some tumors do develop in ovariectomized mice (36), but not in the short term.

The apoptotic indices were evaluated at 3 weeks after hormone stimulation. Apoptotic activity was low ($\leq 1\%$) and was not different with respect to hormone treatment or p53 status (data not shown).

The results of the cytogenetic analyses are shown in Table 1 and Fig. 3. Wild-type normal mammary cells were not examined, because such cells are uniformly diploid and rarely show aberrations (8). The

Table 1 *Cytogenetic analysis of p53 null mammary epithelium*

Group	No. aneuploid (%)	$\bar{X}$ Chromosome number	Total aberrations	Type aberrations*
Untreated	0/50 (0)	39.6	6	1/5
Untreated	2/50 (4)	39.4	3	3/0
Untreated	9/50 (18)	49.2	16	6/10
Pituitary isograft	7/50 (14)	41.4	14	7/7
Pituitary isograft	23/50 (46)	56.7	17	3/14
Estrogen	3/50 (6)	41.8	12	4/8
Progesterone	14/50 (28)	50.6	7	3/4
Progesterone	17/50 (34)	49.2	14	10/4
Tumors (irrad.)	37/50 (74)	67.2	25	19/6
Tumors (unt.)	45/50 (90)	65.9	27	25/2
Tumors (irrad.)	49/50 (98)	59.7	26	8/18
Tumors (irrad.)	49/50 (98)	68.0	10	5/5
Tumors (irrad.)	49/50 (98)	75.8	5	2/3

Abbreviations: irrad, irradiation; unt, untreated.
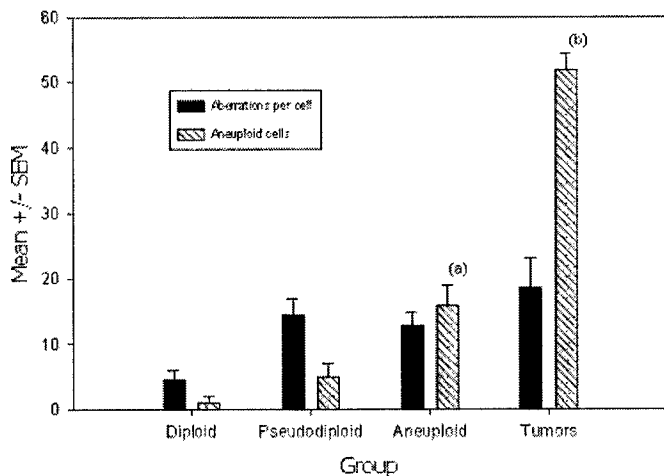* chromosomes/chromatid.

Fig. 3. Cytogenetic analysis of p53-null mammary epithelium. The groups analyzed were untreated p53-null normal ($n = 3$), pituitary isograft-stimulated p53-null normal ($n = 2$), progesterone- or estrogen-treated p53-null normal ($n = 3$), and randomly selected primary tumors ($n = 5$). The p53-null normal cells were collected from treatments described in experiment 1 (Fig. 1). Wild-type normal mammary were not examined because such cells were uniformly diploid. Bars, ±SD. (a, $P < 0.05$ compared with diploid and pseudodiploid; b, $P < 0.05$ compared with aneuploid).

pseudodiploid cell populations were those defined as 41–42 chromosome number. As expected, the number of aneuploid cells increased with hormone stimulation and was greatest in the tumors. The frequency of chromosome aberrations increased slightly in the pseudodiploid cells but did not accumulate to larger numbers in the aneuploid "normal" cells or tumors. This difference was not statistically significant when analyzed by ANOVA. Thus, it appeared that chromatid and chromosome aberrations reflected the underlying state of genetic instability in the p53-null cells but were not correlated directly with aneuploidy. We interpret these data, along with unpublished sister chromatid exchange results, to indicate that the hormonal induction of aneuploidy was not a direct consequence of hormone-induced DNA damage.

The results of the comparative genomic hybridization studies are shown in Fig. 4. The hormone-stimulated (via pituitary isograft) p53-null cells showed an average of 7.3 alterations per sample compared with 2.0 for the hormone-stimulated p53 WT cells. The alter-

ations were distributed randomly over the genome with the exception of a consistent gain in the distal region (H2–3) of mouse chromosome 2 (3/3). The majority of the alterations (18/22) were gains.

The results of the Western blot analysis for mitotic proteins are shown in Fig. 5. Consistent with previous experiments, hormone stimulation increased the level of DNA synthesis to ~8% compared with 2% observed in the transplants in the nonpituitary isograft bearing mice. Several mitotic proteins in their native form either increased from undetectable or very low levels to high levels (separase and securin) or increased in posttranslated modified forms (p55CDC, Cdh1, and Mad2) as a consequence of hormone stimulation. Bub1 was decreased significantly (Fig. 5A). The effect of hormones on mitotic-related proteins appeared to be selective as expression of a number of other proteins involved in various phases of the cell cycle remained unchanged (Fig. 5B). Rad21(M), cyclin E1(G_1-S), Rad51(S), Cdc2(G_2-M), and cyclin B1(G_2-M) protein levels remained at similar levels. The lack of an effect on cohesion Rad21, a sister chromatid cohesion protein, indicates the specificity and selective effect of hormones on this process. In addition, additional increases of separase and Mad2 were detected in p53-null cells compared with p53 WT cells in both untreated transplants (Mad2) and hormone-stimulated transplants (Mad2 and separase; Fig. 5C). Of interest, securin was not increased additionally in hormone-stimulated p53-null cells compared with hormone-stimulated WT cells (Fig. 5D). The quantitative analysis of these changes is shown in Fig. 5D.

To determine whether the increase in protein reflected a direct effect of hormones on gene expression or an indirect effect because of alveolar cell differentiation over the 5-week period, we evaluated the mammary transplants after short-term hormone stimulation. Seven weeks after transplantation, mice were exposed to chronic hormone treatment (50 μg E2 and 20 mg P) via silastic implants, and 8 mice were exposed to blank implants. At 18 and 48 h of hormone stimulation, the transplants were collected, epithelial cell pellets prepared, and RNA isolated. Northern blot analysis revealed marked increases ($\geq$4x) in ESPL1 mRNA at 18 and 48 h posttreatment compared with controls (Fig. 6).

To obtain a more precise picture of the time course of hormone-induced gene transcription of mESPL1, we used an established in vitro model of human breast cells, the MCF7 cancer cell line. This was
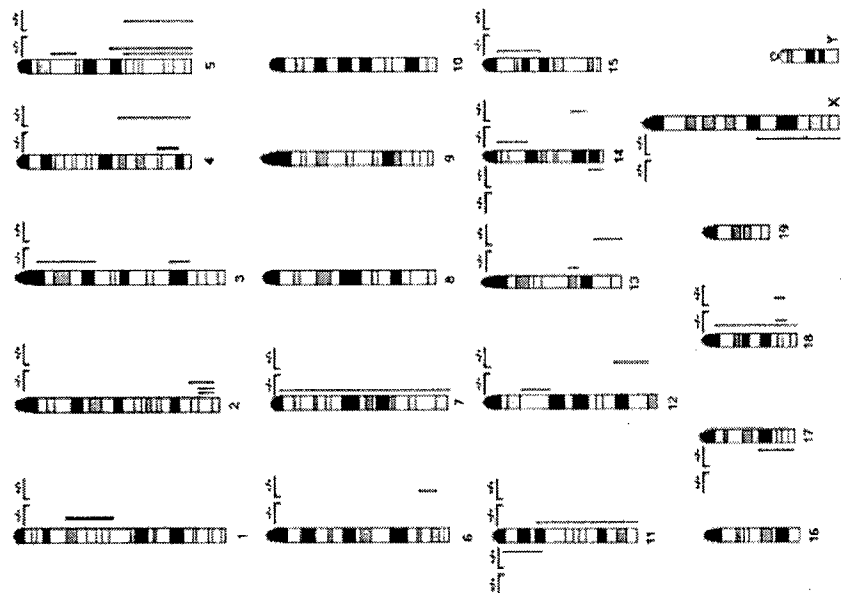

Fig. 4. Karyogram of the DNA copy number changes observed in the p53-null mammary cells obtained from 3 different samples compared with p53 wild mammary cells obtained from 3 different samples. Bars on the left side of the chromosome ideogram indicate losses, and bars on the right side indicate gains. Bold bars on the right side indicate amplifications. For each chromosome, the bars have been grouped to summarize the results of the p53−/− cells and the p53+/+ cells.

A

WT
+ pit

- Separase
- Securin
- p55CDC [Cdc20] [APC activator]
- Cdh1 [APC activator]
- Mad2
- Bub1
- α-Tubulin [Loading Control]

2%   8%   ← Cells in Proliferation

B

WT
+ pit

- Rad21 (M/G1)
- Cyclin B1 (G2/M)
- Cdc2 (G2)
- Rad51 (S)
- Cyclin E1 (G1/S)
- α-Tubulin [Loading Control]

C

WT   p53-/-
+pit   +pit

- Separase
- αTubulin
- Mad2
- αTubulin
- Securin
- αTubulin
- Rad21
- β actin

2% 8% 2% 8% ← Cells in Proliferation

D

- ■ Separase
- □ Mad2
- ▨ Securin
- ▤ Rad21

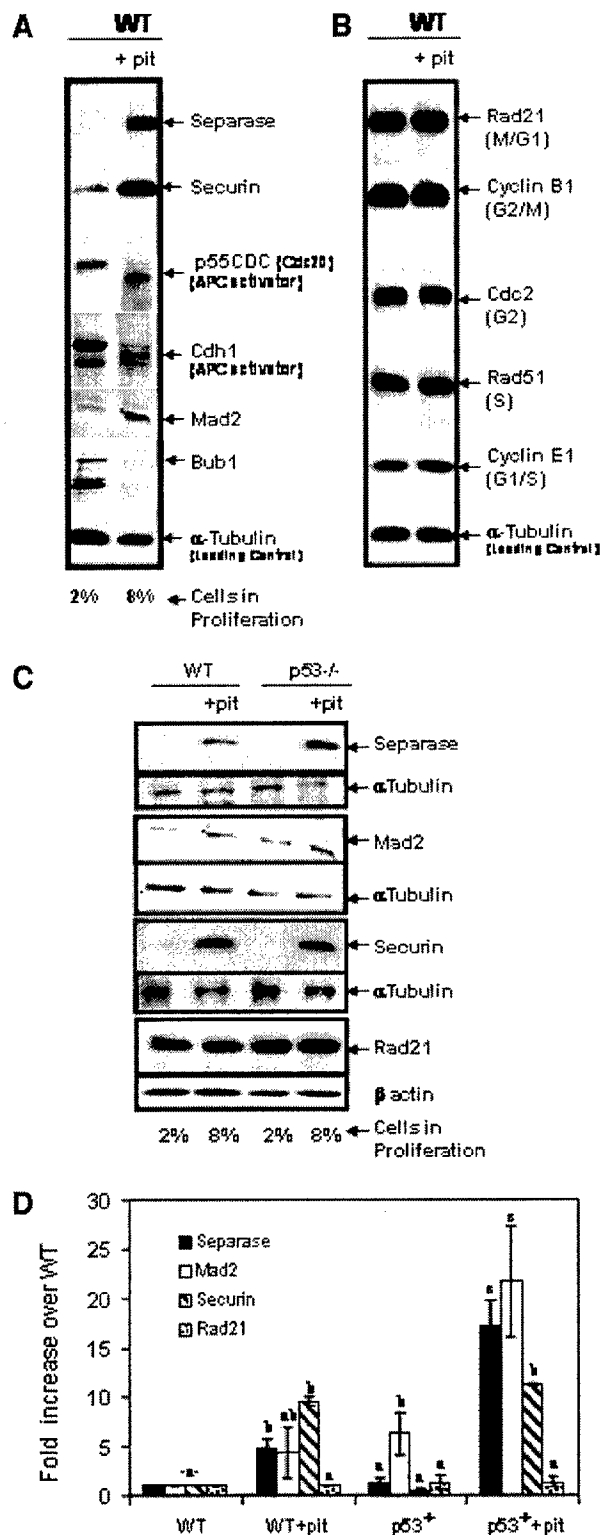Fold increase over WT

WT   WT+pit   p53⁺   p53⁺+pit

Fig. 5. Western blot analysis of the effect of steroid hormone on the expression of mitotic proteins involved in sister chromatid cohesion and separation and spindle damage checkpoint. A, represents the expression of separase, mitotic inhibitor securin, anaphase promoting complex/C regulators p55Cdc and Cdh1, and anaphase promoting complex inhibitor Mad2 and Bub1 in mammary glands with WT p53 in the absence and presence of pituitary (+pit) isograft. B, represents effect of hormones on expression of a number of other proteins involved in various phases of cell cycle control. C, shows the differential expression of separase, Mad2, securin, and Rad21 in p53 WT versus null p53−/− glands. D, represents expression of separase, Mad2, securin, and Rad21 as fold increases over p53 WT glands after normalization to the expression of a housekeeping gene α-tubulin/β-actin to compensate for loading control. Data are the average of the means from two (Mad2 and securin) to four (separase and Rad21) experiments. Individual values were compared using Student's t test. Values with dissimilar symbols are different (P < 0.05). Bars, ±SE.

necessary because mouse mammary cells are notoriously unresponsive to estrogen and progesterone in monolayer cell culture. Fig. 7 shows a time-dependent increase in hESPL1 mRNA and protein levels with hormone treatment. The mRNA reached a maximum 4× increase by 8 h of hormone treatment that persisted for 48 h. Increases in protein started at 8 h with continuing increases at 20 and 48 h.

In view of the hormonal stimulation of separase and Mad2 protein expression (Fig. 5, A and C, and separase mRNA, Figs. 6 and 7), we examined the sequence of the 5' upstream region of both mouse and human ESPL1 (encodes separase protein) and MAD2 genes for potential transcription start sites and potential transcriptional factor binding site (Fig. 8) using bioinformatics tools (35).[10] In mouse ESPL1, we identified a strong promoter sequence with a score of 0.99 (a score of 0.85 has a 0.1–0.4% false positive prediction rate; Fig. 8A). A TATA box (TATAT) is found 30 bp 5' of the putative transcriptional initiation site. Along with a number of putative transcriptional binding sites, two sequences that have 100% homology to the consensus sequence of estrogen responsive element and progesterone responsive element at 203 bp and 93 bp 5' of transcription start sites, respectively, and a sequence that is 90% homology to the consensus sequence p53 transcriptional activation element were identified (Fig. 8A). Sequence analysis also indicated a putative p53 transcriptional repressor element, at position 1636 bp 5' of transcription start sites, that is identical to the consensus sequence. The p53 transcriptional repressor element is a recently identified cis-acting sequence element identified on the basis of its involvement in the suppression of p53-mediated promoter activation (37). Analysis of human ESPL1 sequence also indicated presence of p53, p53 transcriptional repressor element, progesterone responsive element, and estrogen receptor binding elements (data not shown). The presence of the p53 and steroid responsive elements signify a potential transcriptional control of separase expression by p53 and steroids hormones. It is interesting to note that compared with WT glands, p53-null mammary cells have a significantly higher level of Mad2 and a slightly higher separase (Fig. 5D). Analysis of both mouse and human MAD2 promoter sequences (Fig. 8B) indicated the presence of a putative progesterone responsive element, estrogen responsive element, and p53 transcriptional repressor element, but not p53 transcriptional activation element sites.

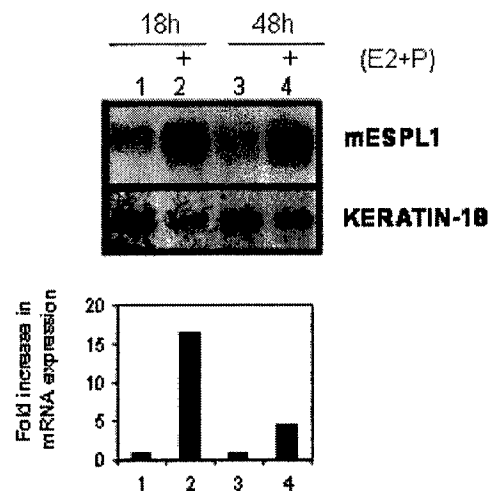The increase in Mad2 levels was initially surprising to us; therefore,

18h   48h
+   +
1   2   3   4   (E2+P)

mESPL1

KERATIN-18

Fold increase in mRNA expression

1   2   3   4

Fig. 6. Transcriptional activation of mESPL1 mRNA by progesterone (P) and estrogen (E2) treatment in p53-null mammary gland cells in vivo. Mammary gland cells were treated in vitro with E2+P for 18 h and 48 h, and Northern blot analyses were performed. Keratin-18 is shown to compare loading. Optical densities of the bands were quantified using ImageQuant software. The quantified mESPL1 mRNA levels were divided by the intensity of the corresponding keratin-18 bands.
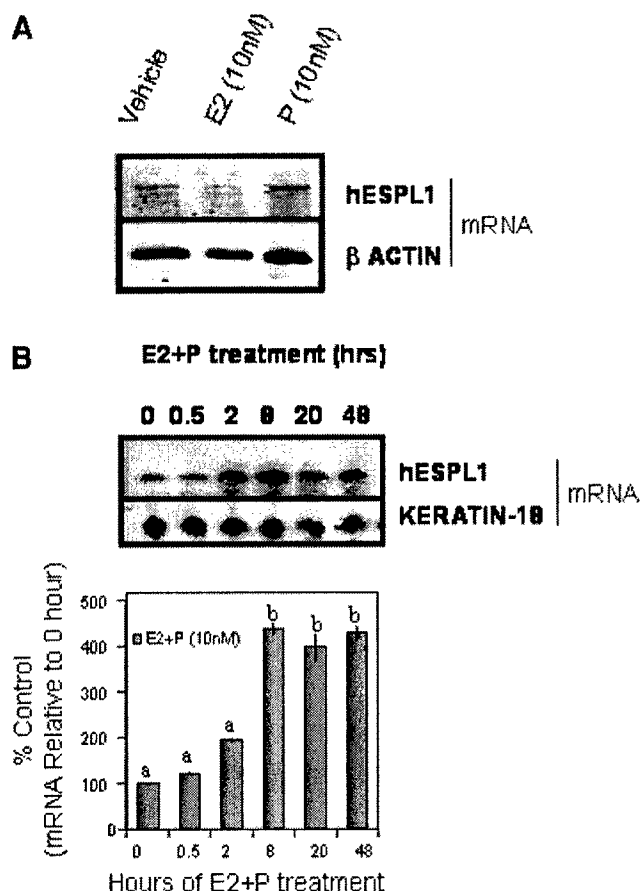
A

B

E2+P treatment (hrs)

Hours of E2+P treatment

Fig. 7. Transcriptional activation of *hESPL1* mRNA by progesterone (*P*) and estrogen (*E2*). Northern blot analysis of *hESPL1* mRNA levels in MCF-7 cells. Cells were seeded in 5% charcoal-stripped serum IMEM for 24 h, seeded in serum-free IMEM for another 48 h, and treated with ethanol (*vehicle*) or P (10 nM), E2 (10 nM; *A*), or E2+P (10 nM each; *B*) in fresh serum-free media as indicated. The mRNA levels were determined as described in the text below. Time course of the combined treatment of E2 and P at a dose of 10 nM each on the expression of *hESPL1* mRNA in MCF7 cells. Keratin-18 is shown as loading control. Bottom panel *B* represents relative *hESPL1* mRNA levels from two independent experiments with respect to the housekeeping gene keratin-18 that was normalized and presented as *% control; bars,* ±SE. Values associated with dissimilar symbols are significantly different ($P < 0.05$ from one another.

we pursued this observation using immunohistochemistry of normal and tumor tissues. Fig. 9 illustrates the patterns of MAD2 expression and localization. Mad2 is detectable at low frequency and intensity of staining in normal cells of p53 WT and p53-null (Fig. 9*A*). However, in small hyperplasias (Fig. 9, *A* and *B*), Mad2 frequency and intensity is markedly increased, and localization in the cytoplasm as well as the nucleus becomes apparent. In tumors, Mad2 continues to be highly expressed, and cytoplasmic localization can be significant (Fig. 9, *C* and *D*).

DISCUSSION

The presence of aneuploidy in tumor cells is undisputed. However, the significance of aneuploidy as an obligatory mechanism of tumorigenesis and tumor progression is controversial (15, 16). In an earlier study, we reported that hormones greatly increased the frequency of aneuploidy in normal mammary cells that had lost the p53 tumor suppressor gene (8). Additionally, these same hormones increased the frequency of tumorigenesis, and the resultant tumors were also highly aneuploid (36). Beyond this initial correlation, the possible mechanisms by which hormones might induce aneuploidy were not addressed. The results described herein address this major question.

First, the results show that the p53-null and p53 WT cells exhibit a similar proliferative response to estrogen and/or progesterone. These results, together with previous results demonstrating a similar degree of dependence on these ovarian hormones for growth in ovariectomized mice as well as for tumor development (36), argue strongly that the cellular responses to these hormones with respect to control of proliferation are normal and should not be considered as dysregulated. Additionally, analysis of the RNA transcriptome demonstrates that the p53-null mammary cell responds normally to these hormones with respect to milk protein synthesis (27). Thus, an altered proliferative response is not likely the cause of the marked increase in aneuploidy.

Second, the hormone-induced aneuploidy in the p53-null cells was not correlated with increases in chromosomal breaks, dicentrics, or translocations, which are markers for DNA damage. The lack of any increase in DNA damage as determined by two different assays (sister chromatid exchange and oxidative damage) also does not support the idea that the hormones were increasing these biochemical events.[11] Previously, we ruled out the mechanism of centrosome duplication (8) as a source of aneuploidy; thus, the data thus far suggest that these two mechanisms (*i.e.,* DNA damage and centrosome duplication) are not important in the hormone-mediated induction of aneuploidy in normal p53-null mammary cells.

Given the above results, we examined the mechanism proposed by Pihan and Doxsey (19) that increased aneuploidy in these cells is a consequence of mitogenesis. Lengauer *et al.* (38) argue that the rate of chromosomal missegregation with normal mitosis is on the order of 1% of mitotic events and that this missegregation would elicit a cell cycle checkpoint, thereby preventing accumulation of aneuploid cells in the organism. However, in the absence of a normal G_2 checkpoint, as in p53-null cells, there would be an accumulation of cells with abnormal mitoses. Although some of these would be nonviable cells, it is likely that viable, aneuploid cells would accumulate in the cell population. An increased frequency of proliferation would shorten the time for aneuploid cells to accumulate in the cell population. This scenario is exactly what is indicated by our results. In the virgin animal, proliferation is low, and the appearance of detectable aneuploid cells increases with host age so that there is no detectable aneuploidy in p53-null cells at 8–14 weeks of age but low levels of aneuploidy at 22–26 weeks of age (8). With hormone-induced increases in proliferation in p53-null cells, there is a marked induction of aneuploidy. Importantly, there is no aneuploidy in p53 WT cells.

These results raise the question whether the absence of p53 confers merely a passive mechanism for generation of aneuploidy or whether p53 is more directly involved by altering the transcriptional regulation or functional activities of genes that are important for proper chromosomal segregation. There have been considerable advances in understanding the genes involved in sister chromatid separation and chromosome segregation (17). The relationship between p53 and the genes involved in regulating chromosome segregation is not well established. The results reported herein indicate that the levels of several proteins important for the regulation of orderly sister chromatid separation are increased in mitosis. More importantly, the levels of two of these proteins (Mad2 and separase) are increased in hormone-treated p53-null cells compared with hormone-treated p53 WT mammary cells. Hormone treatment also increased separase RNA expression. The increase in separase RNA was observed in normal p53-null mouse cells *in vivo* by 18 h and in p53 WT MCF7 human cancer cells *in vitro* by 8 h. These results support the idea that hormones were directly causing an increase in separase gene expression. The significance of the increase in separase is inferred from the knowledge of its

---

[11] Unpublished data.
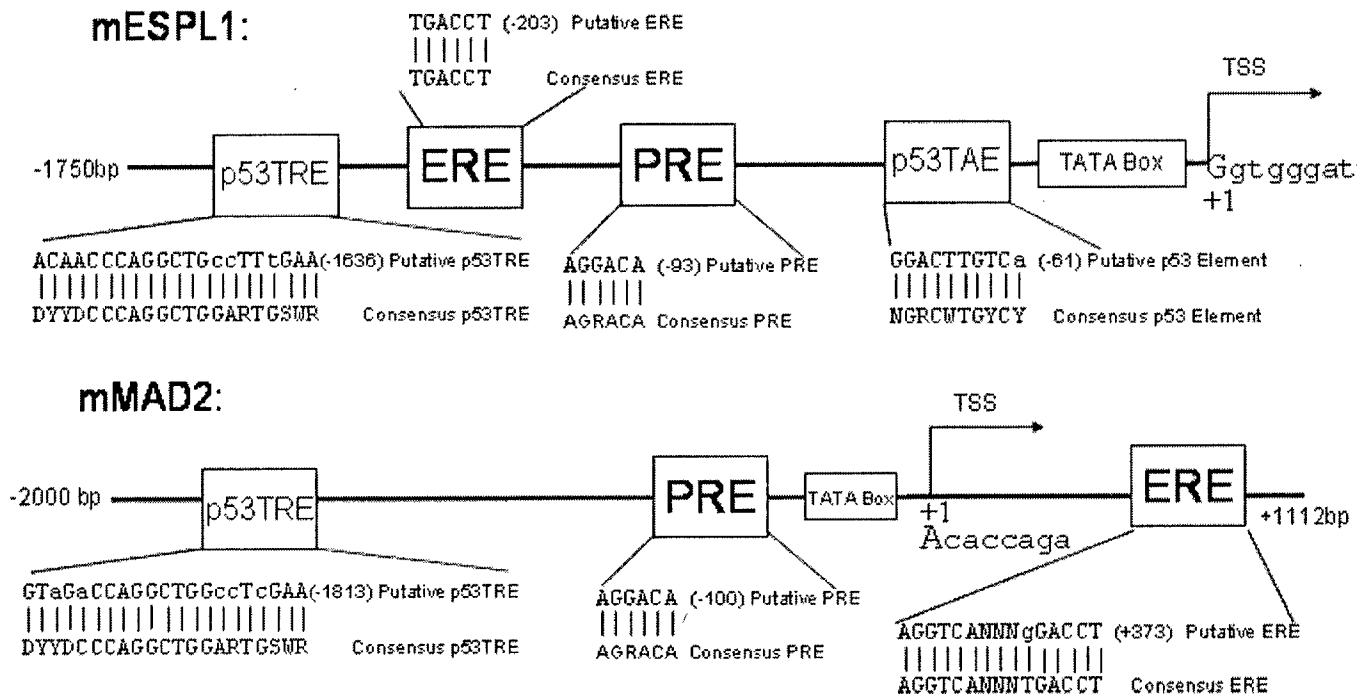
mESPL1:

mMAD2:

Fig. 8. Schematic drawing showing the putative sequence motifs of the separase and Mad2 promoters. *Arrow*, the predicted transcription start site (*TSS*); and C, the +1 position. T ATAT *TATA-box* at −30, putative progesterone responsive element (*PRE*), estrogen responsive element (*ERE*), p53 transcriptional activation element (*p53TAE*) and p53 transcriptional repressor elements (*p53TRE*) are also shown. The following IUPUC-IUB codes for nucleotides were used: R, purine (A or G); Y, pyrimidine (C or T); W(A or T); S(G or C); D (G, A, or T); N, any nucleotides.
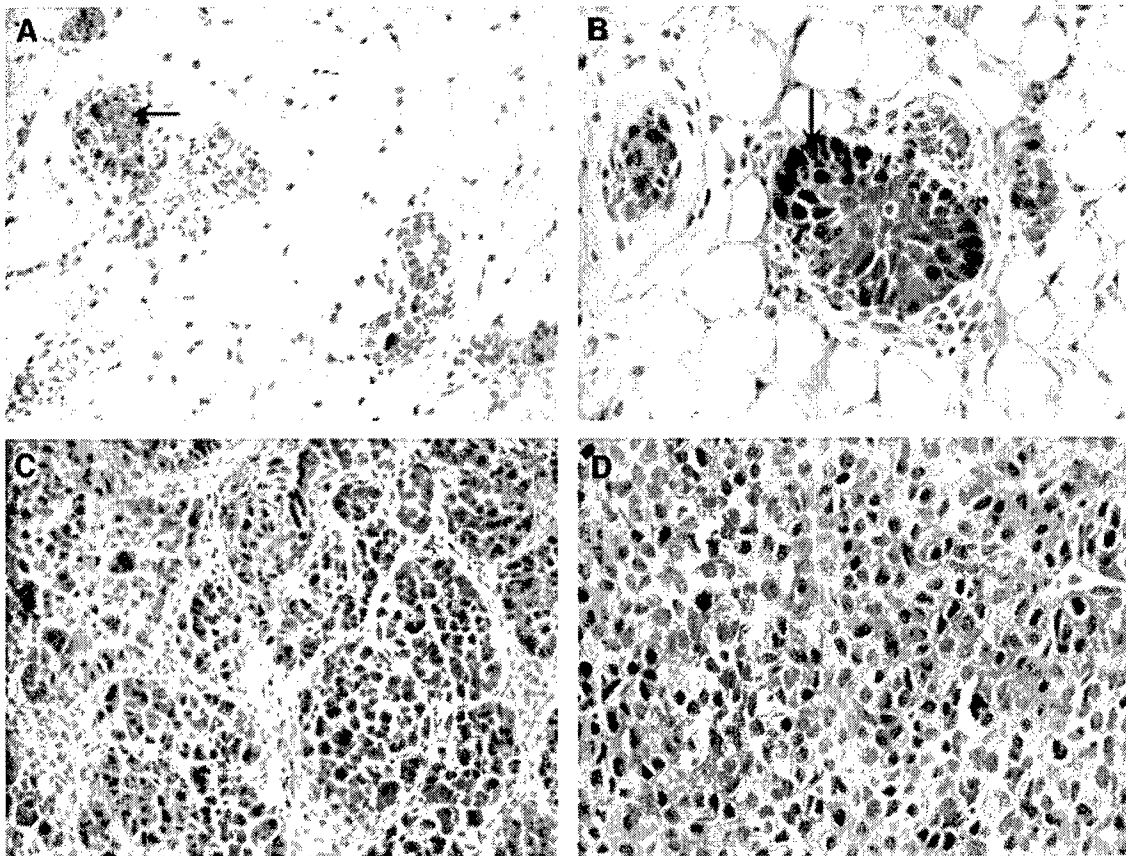

Fig. 9. Mad2 immunohistochemical staining of p53-null normal mammary cells (*A* and *B*), ductal hyperplasia *(arrows* in *A* and *B*), and mammary cancers (*C* and *D*). The staining is low in normal appearing ducts but strongly enhanced in hyperplasias and cancer. The cytoplasmic staining is readily apparent in *D*. Magnification is ×20 (*A* and *C*) and ×40 (*B* and *D*).

function, because separase activity is necessary for sister chromatid separation (17). A direct effect of estrogen on Mad2 gene expression has been reported also by an *in vivo* study in mouse uterus using microarray analysis, where a 6.5-fold increase in Mad2 RNA was reported after estrogen treatment (39).

Interestingly, securin and Rad21 protein levels were not increased in the hormone-stimulated p53-null cells compared with the hormone-stimulated WT cells. Securin is already elevated as a consequence of hormone stimulation; however, Rad21 protein remains at basal levels. If securin and separase are high, one might predict lower levels of Rad21 because of the increased protease activity represented by separase. One explanation for this paradox might be found in the dynamics of Rad21 localization in mammalian cells. The majority of Rad21 dissociates from the centromere in prophase and localizes as unbound protein in the nucleoplasm (40). The cleaved protein from the centromere will represent a small fraction of the total Rad21 pool and is unlikely to alter the signal detected by the antibody on a Western blot. Alternatively, the increased separase protein may represent a catalytically inactive protein. This question remains to be answered.

Why the two proteins (Mad2 and separase) are differentially regulated by p53 is explained by the analysis of the respective promoters of the two genes. Both promoters contained p53 and steroid hormone response elements. The *ESPL1* promoter differed from the MAD2 promoter in the additional presence of a p53 transcriptional activation element. Analysis of p53-regulated gene expression from a published study using oligonucleotide arrays identified MAD2 as one of the genes that is repressed by p53 (41). Previous observations suggest that the p53 transcriptional repressor element sequence can modulate p53-dependent transcriptional activation in a position and promoter-independent manner (37). These results support the hypothesis that in WT mammary cells, p53 can act to dampen steroidal induction of separase and Mad2 gene transcription. In the absence of p53 function, steroid hormones manifest their uninhibited effects by significant induction of *ESPL1* and MAD2 gene expression that facilitates aneuploidy. The physiological significance and mechanism of p53 repression and its coregulation, if any, with the p53 activation binding elements is yet to be elucidated.

The significance of elevated Mad2 is more difficult to understand because this protein functions to inhibit the anaphase promoting complex, and the functional activity of the latter complex is necessary for releasing separase activity (17). Haploinsufficiency of Mad2 results in chromosome instability (42). Also, the appropriate functioning of the spindle checkpoint requires a critical ratio of Mad1 and Mad2 to ensure a pool of Mad1-free Mad2 (43). An excess of Mad2 as well as insufficient Mad2 might result in an altered spindle checkpoint. Another possibility is that the increased form of Mad2 is an inactive form, but this remains to be tested experimentally. Finally, it is possible that the increased levels of Mad2 are only related indirectly to the increased aneuploidy but rather have effects on other cellular functions (44–46). It has been reported recently that increased levels of Mad2 are present in gastric tumors (47) and ovarian tumors (48). The results reported herein demonstrated increased levels of Mad2 in mammary hyperplasias and tumors. Additionally, the localization of Mad2 in these lesions was both nuclear and cytoplasmic compared with just nuclear in normal cells. These results along with reported interactions of Mad2 with proteins thought to be unrelated to control of mitosis (44–46) suggest that Mad2 affects multiple cellular functions. In either event, the observation that proteins involved in regulation of sister chromatid separation are altered in p53-null cells provide a mechanism that is consistent with aneuploidy occurring in the absence of other suggested mechanisms (*i.e.,* DNA damage and centrosome duplication).

Are the effects of hormones more encompassing than just increased levels of separase and Mad2 driving chromosome missegregation? We have tried to assess this question using two different approaches. First, analyzing the pattern of chromosomal gains and losses by comparative genomic hybridization revealed one consistent chromosomal alteration in hormone-stimulated p53-null cells compared with hormone p53 stimulated WT cells. The most consistent change occurred in the distal region of chromosome 2, a region in the mouse harboring genes such as MMP9, kinesin, β-2 microglobulin, and intracisternal A particles. This region is syntenic to human chromosome 20q11.21 and 20q13.32. Genes of interest in this region include aurora kinase A, breast carcinoma amplified sequence 1, ubiquitin-related protein sumo-1, protein tyrosine phosphatase 1B, and CCAAT/enhancer binding protein β. We are examining the expression of some of these genes at the protein level; namely, aurora kinase A and CCAAT/enhancer binding protein β.

The second approach used was serial analysis of gene expression, which showed alterations in ~1% of the transcriptome of the hormone-stimulated p53-null mammary cells (27). These genes included known p53-regulated genes such as gelsolin, Gadd45b, and Igfbp5, and other genes not thought to be directly regulated by p53, such as intracisternal A particles, MMP9, β-2 microglobulin, and wdnm1 (27). The first three of these genes are located on the distal arm of chromosome 2. The role of any of these genes in regulation in sister chromatid separation and/or mitosis is not suspected.

The amplification of intracisternal A particles, a gene that is a transposon, suggests another possibility for generating aneuploidy and/or increased RNA expression of the genes. The gain of this region was also observed as increases in intracisternal A particles by electron microscopy.[12] The increase in transposon activity has been shown to activate specific gene functions in other mouse models of mammary tumorigenesis (49, 50).

Based on the current accumulated data, we are proposing that hormone facilitation of aneuploidy in p53-null mammary epithelial cells occurs by several mechanisms. First, we suggest that hormones have an indirect role in the induction of aneuploidy by markedly increasing the mitotic frequency of these normal cells and a direct role by increasing the expression levels of proteins regulating chromosome segregation. We hypothesize that the absence of p53 function results in both an aberrant separase activity and an aberrant G_2 checkpoint that together allows the accumulation of cells with aneuploidy as a function of time and mitotic frequency. The presence of aneuploidy has an indirect effect on tumorigenesis by increasing stochastically the frequency of altered expression of genes involved in growth regulation and invasiveness. Second, we speculate that hormones specifically increase expression of genes localized in the distal region of chromosome 2, which contains genes related to control of chromosome segregation (*e.g.,* aurora kinase A), as well as genes involved in premalignant progression (*e.g.,* CCAAT/enhancer binding protein β and SUMO-1). Future experiments will test these hypotheses.

ACKNOWLEDGMENTS

REFERENCES

1. Fukasawa K, Choi T, Kuriyama R, Rulong S, Vande Woude GF. Abnormal centrosome amplification in the absence of p53. Science (Wash DC) 1996;271:1744–7.
2. Tarapore P, Fukasawa K. p53 mutation and mitotic infidelity. Cancer Investig 2000;18:148–55.

---

[12] D. Medina, unpublished result.

3. Chiba S, Okuda M, Mussman JG, Fukasawa K. Genomic convergence and suppression of centrosome hyperamplification in primary p53-/- cells in prolonged culture. Exp Cell Res 2000;258:310–21.

4. Donehower LA, Godley LA, Aldaz CM, et al. Deficiency of p53 accelerates mammary tumorigenesis in Wnt-1 transgenic mice and promotes chromosomal instability. Genes Dev 1995;9:882–95.

5. Shao C, Deng L, Henegariu O, et al. Chromosome instability contributes to loss of heterozygosity in mice lacking p53. Proc Natl Acad Sci USA 2000;97:7405–10.

6. Bunz F, Fauth C, Speicher MR, et al. Targeted inactivation of p53 in human cells does not result in aneuploidy. Cancer Res 2002;62:1129–33.

7. Lu X, Magrane G, Yin C, et al. Selective inactivation of p53 facilitates mouse epithelial tumor progression without chromosomal instability. Mol Cell Biol 2001; 21:6017–30.

8. Goepfert TM, McCarthy M, Kittrell FS, et al. Progesterone facilitates chromosome instability (aneuploidy) in p53 null normal mammary epithelial cells. FASEB J 2000;14:2221–9.

9. Auer GU, Heselmeyer KM, Steinbeck RG, Munck-Wikland E, Zetterberg AD. The relationship between aneuploidy and p53 overexpression during genesis of colorectal adenocarcinoma. Virchows Arch 1994;424:343–7.

10. Campomenosi P, Assereto P, Bogliolo M, et al. p53 mutations and DNA ploidy in colorectal adenocarcinomas. Anal Cell Pathol 1998;17:1–12.

11. Duesberg P, Rasnick D. Aneuploidy, the somatic mutation that makes cancer a species of its own. Cell Motil Cytoskeleton 2000;47:81–107.

12. Duesberg P, Li R, Rasnick D, et al. Aneuploidy precedes and segregates with chemical carcinogenesis. Cancer Genet Cytogenet 2000;119:83–93.

13. Li JJ, Papa D, Davis JF, et al. Ploidy differences between hormone- and chemical carcinogen-induced rat mammary neoplasms: comparison to invasive human ductal breast cancer. Mol Carcinog 2002;33:56–65.

14. Li JJ, Li SA. Causation and prevention of solely estrogen-induced oncogenesis: similarities to human ductal breast cancer. Adv Exp Med Biol 2003;532:195–207.

15. Li R, Sonik A, Stindl R, Rasnick D, Duesberg P. Aneuploidy vs. gene mutation hypothesis of cancer: recent study claims mutation but is found to support aneuploidy. Proc Natl Acad Sci USA 2000;97:3236–41.

16. Zimonjic D, Brooks MW, Popescu N, Weinberg RA, Hahn WC. Derivation of human tumor cells in vitro without widespread genomic instability. Cancer Res 2001;61: 8838–44.

17. Nasmyth K. Segregating sister genomes: The molecular biology of chromosome separation. Science (Wash DC) 2002;297:559–65.

18. Lingle WL, Barrett SL, Negron VC, et al. Centrosome amplification drives chromosomal instability in breast tumor development. Proc Natl Acad Sci USA 2002;99: 1978–83.

19. Pihan GA, Doxsey SJ. The mitotic machinery as a source of genetic instability in cancer. Semin Cancer Biol 1999;9:289–302.

20. Jallepalli PV, Lengauer C. Chromosome segregation and cancer: cutting through the mystery. Nat Rev Cancer 2001;1:109–17.

21. Cavalieri E, Frenkel K, Liehr JG, Rogan E, Roy D. Estrogens as endogenous genotoxic agents–DNA adducts and mutations. J Natl Cancer Inst Monogr 2000;27: 75–93.

22. Liehr JG. Genotoxicity of the steroidal oestrogens oestrone and oestradiol: possible mechanism of uterine and mammary cancer development. Hum Reprod Update 2001;7:273–81.

23. Jerry DJ, Kittrell FS, Kuperwasser C, et al. A mammary-specific model demonstrates the role of the p53 tumor suppressor gene in tumor development. Oncogene 2000; 19:1052–8.

24. Kuperwasser C, Hurlburt GD, Kittrell FS, et al. Development of spontaneous mammary tumors in BALB/c p53 heterozygous mice. Am J Pathol 2000;157:2151–9.

25. Medina D, Kittrell FS, Shepard A, et al. Biological and genetic properties of the p53 null preneoplastic mammary epithelium. FASEB J 2002;16:881–3.

26. Jerry DJ, Kuperwasser C, Downing SR, et al. Delayed involution of the mammary epithelium in BALB/c-p53null mice. Oncogene 1998;17:2305–12.

27. Aldaz CM, Hu Y, Daniel R, et al. Serial analysis of gene expression in normal p53 null mammary epithelium. Oncogene 2002;21:6366–76.

28. Christon K, Swanson SM, Guzman RC, et al. Kinetics of mammary epithelial cell proliferation in pituitary isografted BALB/c mice. Carcinogenesis (Lond) 1993;14: 2019–25.

29. Said TK, Conneely O, Medina D, O'Malley B, Lydon J. Progesterone in addition to estrogen induces cyclin D1 expression in mammary epithelial cells in vivo. J Endocrinol 1997;138:3933–9.

30. Murphy K, Kittrell FS, Gay J, et al. Bcl-2 expression delays mammary tumor development in dimethylbenz(α)anthracene-treated transgenic mice. Oncogene 1999; 18:6597–604.

31. Simbulan-Rosenthal CM, Haddad BR, Rosenthal DS, et al. Chromosomal aberrations in PARP-/- mice and genome stabilization in immortalized cells by reintroduction of PARP cDNA. Proc Natl Acad Sci USA 1999;96:13191–6.

32. Figueiredo BC, Stratakis CA, Sandrini R, et al. Comparative genomic hybridization (CGH) analysis of adrenocortical tumors of childhood. J Clin Endocrinol Metab 1999;84:1116–21.

33. Pati D, Zhang N, Plon SE. Linking sister chromatid cohesion and apoptosis: role of Rad 21. Mol Cell Biol 2002;22:8267–77.

34. Medina D, Kittrell FS. Establishment of mouse mammary cell lines. In: Ip MM, Asch BB, editors. Methods in mammary gland biology and breast cancer research. New York: Kluwer Academic Press; 2000. p. 137–45.

35. Quandt K, Frech K, Karas H, Wingender E, Werner T. MatInd and MatInspector: new fast and versatile tools for detection of consensus matches in nucleotide sequence data. Nucleic Acids Res 1995;23:4878–84.

36. Medina D, Kittrell FS, Shepard A, et al. Hormone dependence in premalignant mammary progression. Cancer Res 2003;63:1067–72.

37. Wong J, Li PX, Klamut HJ. A novel p53 transcriptional repressor element (p53TRE) and the asymmetrical contribution of two p53 binding sites modulate the response of the placental transforming growth factor-beta promoter to p53. J Biol Chem 2002; 277:26699–707.

38. Lengauer C, Kinzler KW, Vogelstein B. Genetic instability in colorectal cancers. Nature (Lond) 1997;386:623–7.

39. Reese J, Das SK, Paria BC, et al. Global gene expression analysis to identify molecular markers of uterine receptivity and embryo implantation. J Biol Chem 2001;276:44137–45.

40. Waizenegger IC, Hauf S, Meinke A, Peters JM. Two distinct pathways remove mammalian cohesion from chromosome arms in prophase and from centromeres in anaphase. Cell 2000;103:399–410.

41. Zhao R, Gish K, Murphy M, et al. Analysis of p53-regulated gene expression patterns using oligonucleotide arrays. Genes Dev 2000;14:981–93.

42. Michel LS, Liberal V, Chatterjee A, et al. MAD2 haplo-insufficiency causes premature anaphase and chromosome instability in mammalian cells. Nature (Lond) 2001; 409:355–9.

43. Chung E, Chen RH. Spindle checkpoint requires mad1-bound and mad1-free mad2. Mol Biol Cell 2002;13:1501–11.

44. O'Neill TJ, Zhu Y, Gustafson TA. Interaction of MAD2 with the carboxyl terminus of the insulin receptor but not with the IGFIR. Evidence for release from the insulin receptor after activation. J Biol Chem 1997;272:10035–40.

45. Poelzl G, Kasai Y, Mochizuki N, et al. Specific association of estrogen receptor beta with the cell cycle spindle assembly check-point protein, MAD2. Proc Natl Acad Sci USA 2000;97:2836–9.

46. Takeda M, Dohmae N, Takio K, Arai K, Watanabe S. Cell cycle-dependent interaction of Mad2 with conserved Box1/2 region of human granulocyte-macrophage colony-stimulating factor receptor common betac. J Biol Chem 2001;276:41803–9.

47. Tanaka K, Nishioka J, Kato K, et al. Mitotic checkpoint protein hsMAD2 as a marker predicting liver metastasis of human gastric cancers. Jpn J Cancer Res 2001;92: 952–8.

48. Wang X, Jin D-Y, Ng RWM, et al. Significance of MAD2 expression to mitotic checkpoint control in ovarian cancer cells. Cancer Res 2002;62:1662–8.

49. Asch BB. Tumor viruses and endogenous retrotransposons in mammary tumorigenesis. J Mammary Gland Biol Neoplasia 1996;1:49–60.

50. Van Houten JN, Asch HL, Asch BB. Cloning and characterization of ectopically expressed transcripts from actin-binding protein MIPP in mouse mammary carcinomas. Oncogene 2001;40:5366–72.